THE ASTROPHYSICAL JOURNAL, 464:286–305, 1996 June 10


# X-RAY–EMITTING T TAURI STARS IN THE L1551 CLOUD

LEE CARKNER AND ERIC D. FEIGELSON
Department of Astronomy and Astrophysics, Pennsylvania State University, University Park, PA 16802
KATSUJI KOYAMA
Department of Physics, Kyoto University, Kyoto, Japan
THIERRY MONTMERLE
Service d'Astrophysique, Centre d'Études de Saclay, Gif-sur-Yvette 91101 France
AND
I. NEILL REID
Palomar Observatory, 105-24, California Institute of Technology, Pasadena, CA 91125
*Received 1995 July 26; accepted 1995 December 28*

## ABSTRACT

Low-mass pre–main-sequence stars in the nearby Lynds 1551 star-forming cloud are studied with the *ROSAT* and *ASCA* X-ray satellites. An 8 ks *ROSAT* image reveals 38 sources including seven well-known T Tauri stars, two likely new weak-lined T Tauri stars, five potential new weak-lined T Tauri stars, one young B9 star, and the remaining sources are unrelated to the cloud or poorly identified. A 40 ks *ASCA* image of the cloud detects seven of the *ROSAT* sources.

Spectral fitting of the brighter X-ray–emitting stars suggests the emission is produced in either a multi-temperature plasma, with temperatures near 0.2 and 1 keV, or a single-temperature plasma with low metal abundances. XZ Tau, a young classical T Tauri star, is much stronger in *ASCA* than *ROSAT* observations, showing a harder (1.5–2.0 keV) component. Timing analysis reveals all but one of the T Tauri stars are variable on timescales ranging from 1 hr to 1 year. A powerful flare, emitting $3 \times 10^{34}$ ergs within a 40 minute rise and fall, was observed by *ASCA* on the weak-lined T Tauri star V826 Tau. The event was preceded and followed by constant quiescent X-ray emission. The extreme classical T Tauri star XZ Tau was also caught during both high and low states, varying by a factor of 15 between the *ASCA* and *ROSAT* observations. Neither of the luminous infrared embedded protostars L1551 IRS 5 or L1551NE were detected by *ROSAT* or *ASCA*.

*Subject headings:* ISM: individual (L1551) — stars: activity — stars: pre–main-sequence — X-rays: stars

## 1. INTRODUCTION

The phase of low-mass stellar evolution directly preceding the long-lived main-sequence, or T Tauri phase, was discovered by Joy (1942) by examining the spectra of variable stars in and around dark clouds. T Tauri stars have emerged from their obscuring dusty cloud, are contracting along the convective Hayashi tracks, and show normal stellar photospheres with temperatures around 3000–4000 K. Some, but not all, T Tauri stars maintain a dusty circumstellar disk, which produces a strong infrared-millimeter excess. Interaction between the star and disk, which may involve accretion and/or wind ejection, produces the broad optical emission lines and ultraviolet veiling characteristic of "classical T Tauri" (CTT) stars. "Weak-lined T Tauri" (WTT) stars generally lack the disk or possess optically thin disks that do not interact with the star and consequently lack the associated emission lines and continuum excesses. T Tauri stars are thought to evolve from the CTT to the WTT phase as the disk dissipates, though some WTT stars are very young (Bertout 1989; Appenzeller & Mundt 1989).

Hα and infrared surveys have been the traditional means of identifying CTT stars but are inefficient in locating WTT stars. Most WTT stars have been found in soft X-ray observations of nearby star-forming clouds using the *Einstein Observatory* and *ROSAT*. These data reveal strong ($10^{29}$–$10^{31}$ ergs $s^{-1}$ or $10^2$–$10^4$ times contemporary solar levels) soft X-ray emission from many CTT stars and even larger populations of WTT stars. Studies of X-rays from T Tauri stars have been made in the Taurus-Auriga (Feigelson et al. 1987; Walter et al. 1988; Strom & Strom 1994; Neuhäuser et al. 1995a), Orion (Gagné & Caillault 1994), Chamaeleon I (Feigelson et al. 1993, hereafter FCMG), ρ Ophiuchi (Montmerle et al. 1983; Koyama et al. 1994; Casanova et al. 1995), and other star-forming regions. The X-ray emission is usually modeled as a ~1 keV optically thin plasma, though observations with the *Tenma*, *Ginga*, and *ASCA* satellites indicate that a few T Tauri stars have large emission measures at higher temperatures (Koyama 1987, Koyama et al. 1992, 1994).

The X-ray emission is attributed to enhanced solar-type magnetic activity; that is, optically thin plasma trapped in closed magnetic structures and heated by magnetic processes such as reconnection. WTT stars exhibit a wealth of indicators for strong magnetic activity including strong variability in the X-ray emission on timescales of minutes to days, cool photospheric starspots covering 5%–40% of the surface, enhanced chromospheric lines, and powerful non-thermal radio continuum flares in some stars. CTT stars may share this magnetic activity, though the indicators are confused by the complex star-disk interactions. The magnetic properties of T Tauri stars are reviewed by Feigelson, Giampapa, & Vrba (1991) and Montmerle et al. (1993). T Tauri X-rays may significantly affect the ionization of molecular cloud cores and thus the physics of star formation (Silk & Norman 1985; Silk 1995).

We study here X-ray emission from stars around Lynds 1551, a well-studied cloud in the Taurus-Auriga star-forming region. The cloud subtends less than 1 $deg^2$ and

contains 17 previously known T Tauri stars and a young B9 emission-line star. It lies behind a portion of the Hyades star cluster, the members of which can also be X-ray luminous. *Einstein* observations of the cloud have detected 15 X-ray sources, including seven T Tauri stars (Feigelson & DeCampli 1981; Feigelson et al. 1987), and the region was detected as the source 1H 0427+177 in the 2–6 keV band during the *HEAO 1* all-sky survey (Wood et al. 1984). It is the site of the first X-ray–discovered WTT stars (Feigelson & Kriss 1981). L1551 also has remarkable outflows, including the bipolar molecular flows from the embedded infrared sources L1551 IRS 5 and L1551NE, and a complex of jets and Herbig-Haro objects emerging from the extremely young CTT stars HL Tau and XZ Tau. The cloud has been thoroughly surveyed for Hα emission stars (Cudworth & Herbig 1979; Feigelson & Kriss 1983) and proper-motion cloud members (Jones & Herbig 1979; Gomez et al. 1992). Altogether, L1551 may have the most intensively characterized pre–main-sequence population of any star-forming cloud. The L1551 cloud is assumed to lie at 140 pc, the same distance as other Taurus-Auriga clouds (Kenyon, Dobrzycka, & Hartmann 1994).

The observations reported here were made in two X-ray bands: the soft 0.1–2.5 keV band of the *ROSAT* satellite and the harder 0.5–10 keV band of the *ASCA* satellite. The *ROSAT* observations provide an order-of-magnitude improvement in sensitivity and spatial resolution compared to earlier *Einstein* observations, revealing over twice as many faint X-ray sources. *ASCA*'s sensitivity to hard X-rays enables the detection of deeply embedded sources, including protostars. The broadband coverage and high spectral resolution of the *ASCA* detectors also permit detailed spectral modeling. This proved to be particularly valuable during a powerful flare observed in the X-ray–discovered WTT star V826 Tau. Thus, *ROSAT* provides an independent census of T Tauri stars, with potential implications for the cloud's star formation efficiency and initial mass function, while *ASCA* provides unique information into the astrophysics of T Tauri X-ray emission.

The observations are described in § 2, stellar identifications and properties are discussed in § 3, X-ray properties are discussed in §§ 4–6, and discussion follows in § 7.

## 2. OBSERVATIONAL DATA

### 2.1. *ROSAT Observations*

On 1993 February 21 and 24, the L1551 cloud was observed with the *ROSAT* Position Sensitive Proportional Counter (PSPC) B for a total of 7724 s (2.15 hr) on target. The instrument is described by Pfeffermann et al. (1986). The *ROSAT* field is a 2° diameter circle centered on the cloud, which fits within the 40′ diameter inner region of the detector, where the point-spread function is narrow. A diagram of the cloud and its previously known pre–main-sequence stars, centered on the PSPC pointing direction, is shown in Figure 1. The PSPC image is shown in Figure 2.

Our source detection and analysis procedure follows that described in a similar study of the Chamaeleon I star-forming cloud (FCMG). A preliminary list of 34 sources was obtained from the Standard Analysis Software System (SASS), which uses maximum-likelihood source existence criteria applied to three spectral bands using two different background estimation procedures (Cruddace, Hasinger, & Schmitt 1988). We reject five of these sources because of low signal-to-noise ratio (S/N ≤ 3.5) with respect to a local background. Visual examination of the smoothed contour map (Fig. 2*b*), followed by calculation of S/N, revealed nine significant sources that were not detected by the SASS software. The resulting total of 38 X-ray sources are shown in Figure 2*b* and are listed in Table 1 with the prefix "L1551X" representing "L1551 X-ray" source.

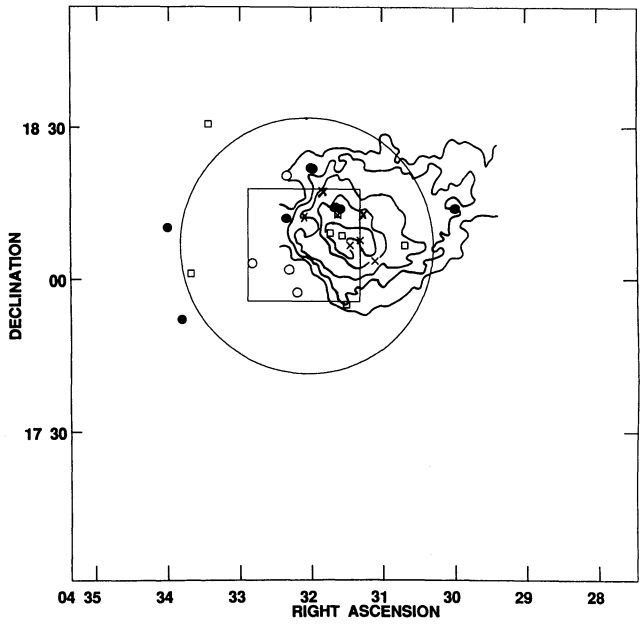


FIG. 1.—Diagram of the L1551 cloud and the reported X-ray observations. Contours represent intensity of CO molecular emission from Moriarty-Schieven & Snell (1988), open circles are WTT stars, filled circles are CTT stars from the catalog of Herbig & Bell (1988), open squares are embedded infrared sources, and crosses are Herbig-Haro objects from the catalog of Reipurth (1994). The diagram is centered on the *ROSAT* PSPC field, and the *ASCA* GIS (*circle*) and *ASCA* SIS (*square*) fields of view are indicated. Axes in Figs. 1–4 are in J2000.

The source positions determined by the SASS can have a boresight error of a few arcseconds, which can be corrected by measuring the systematic offset between the X-ray sources and the known locations of their optical counterparts. Restricting the calculation to seven sources with precise X-ray centroids and unambiguous stellar identifications, the true positions are found to be 2.″9 west and 5.″6 north of the SASS positions. Table 1 lists these boresight-corrected positions, as well as off-axis distance ($\theta$), background-corrected count rate in the 0.1–2.5 keV band, and S/N ratio measured by us with respect to the local background. Positional uncertainties are taken from the SASS results, but we adopt a minimum systematic uncertainty of 4″ in the inner region of the detector ($\theta < 20'$) and large systematic uncertainties ($\pm 30''$ for $\theta < 30'$ and $\pm 60''$ for $\theta > 30'$) because of the poor off-axis resolution of the *ROSAT* mirror. In addition, the table provides *Einstein* Imaging Proportional Counter (IPC) count rates and offsets ($\phi$) in arcseconds from the corresponding *ROSAT* sources, derived from the *Einstein* study of Feigelson et al. (1987). A range of *Einstein* count rates is shown for variable sources. *Einstein* detected fewer than half of the sources found by *ROSAT*, partly because of lower sensitivity and partly because of confusion of closely separated sources.

### 2.2. *ASCA Observations*

The *Advanced Satellite for Cosmology and Astrophysics* (*ASCA*) is composed of four nested foil X-ray telescopes,

1996ApJ...464..286C

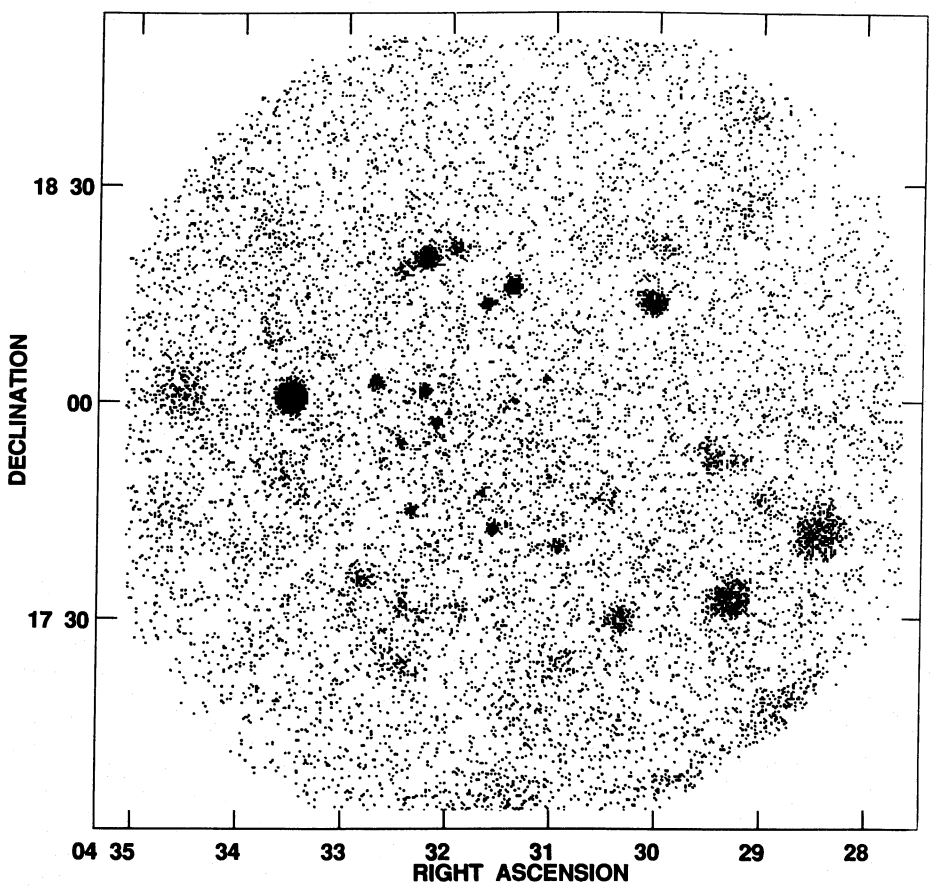


FIG. 2a

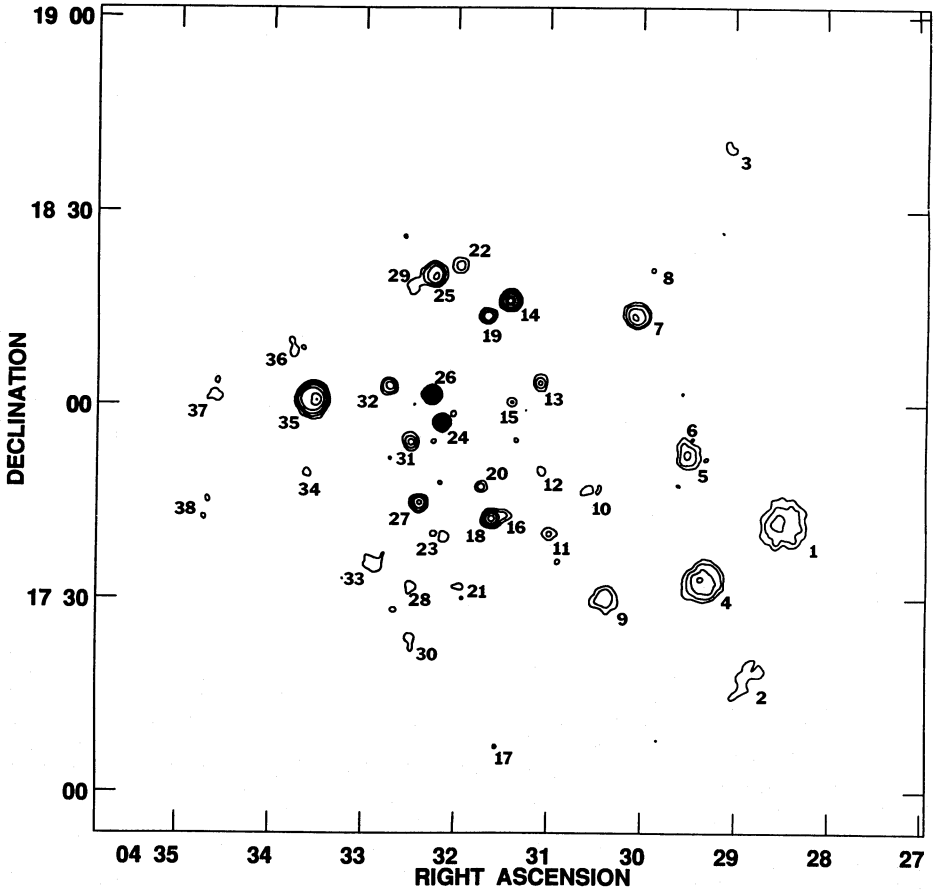


FIG. 2b

FIG. 2.—*ROSAT* PSPC observation of the L1551 cloud. (*a*) Raw image showing individual X-ray and background events. (*b*) Contour map after smoothing with a 1′ FWHM Gaussian kernel. Surface density levels are 0.25, 0.5, 1, 3, 6, 9, and 12 events pixel$^{-1}$. Sources are labeled with L1551X numbers given in Table 1.

TABLE 1

*ROSAT* SOURCES NEAR THE L1551 CLOUD

| L1551X SOURCE | R.A. (2000) | DECL. (2000) | ERROR | $\theta$ | COUNT RATE ($ks^{-1}$) | S/N | HR 1 | ERROR | HR 2 | ERROR | *Einstein* IPC Count Rate | *Einstein* IPC $\phi$ |
|---|---|---|---|---|---|---|---|---|---|---|---|---|
| 1 | $4^h28^m35^s.6$ | 17°41′42″ | 60″ | 43′ | 55 | 22.6 | −0.13 | 0.04 | −0.01 | 0.05 | ... | ... |
| 2 | 4 28 52.3 | 17 18 47 | 60 | 53 | 24 | 7.1 | −0.32 | 0.04 | −0.01 | 0.07 | ... | ... |
| 3 | 4 29 01.2 | 18 38 01 | 60 | 53 | 16 | 4.3 | ... | ... | ... | ... | ... | ... |
| 4 | 4 29 20.3 | 17 32 34 | 60 | 39 | 108 | 23.9 | −0.21 | 0.04 | −0.16 | 0.06 | 52 | 2″ |
| 5 | 4 29 29.6 | 17 52 25 | 30 | 28 | 54 | 15.1 | −0.37 | 0.07 | −0.05 | 0.13 | 14 | 22 |
| 6 | 4 29 33.3 | 17 54 11 | 30 | 27 | 11 | 6.2 | ... | ... | ... | ... | ... | ... |
| 7 | 4 30 05.1 | 18 13 51 | 30 | 25 | 33 | 17.7 | 0.85 | 0.04 | 0.19 | 0.05 | 50 | 5 |
| 8 | 4 29 59.8 | 18 21 51 | 30 | 31 | 17 | 3.8 | ... | ... | ... | ... | ... | ... |
| 9 | 4 30 23.4 | 17 30 04 | 60 | 31 | 45 | 13.9 | −0.04 | 0.08 | −0.20 | 0.10 | ... | ... |
| 10 | 4 30 36.1 | 17 46 42 | 11 | 16 | 3.6 | 4.1 | 0.69 | 0.26 | 0.40 | 0.24 | ... | ... |
| 11 | 4 30 59.5 | 17 40 11 | 8 | 19 | 8.0 | 5.0 | 1.00 | 0.11 | 0.48 | 0.14 | ... | ... |
| 12 | 4 31 04.1 | 17 49 46 | 6 | 9 | 2.0 | 3.5 | 0.81 | 0.37 | −0.28 | 0.31 | ... | ... |
| 13 | 4 31 05.9 | 18 03 29 | 4 | 7 | 9.3 | 8.5 | −0.20 | 0.12 | 0.05 | 0.18 | ... | ... |
| 14 | 4 31 25.5 | 18 16 15 | 4 | 19 | 151 | 25.4 | 0.79 | 0.03 | 0.14 | 0.04 | 45 | 26 |
| 15 | 4 31 24.1 | 18 00 28 | 5 | 3 | 3.1 | 4.1 | 1.00 | 0.18 | 0.05 | 0.22 | ... | ... |
| 16 | 4 31 28.9 | 17 43 08 | 6 | 15 | 5.5 | 5.4 | −0.27 | 0.17 | 0.15 | 0.27 | ... | ... |
| 17 | 4 31 28.9 | 17 05 21 | 60 | 52 | 29 | 3.9 | −0.20 | 0.05 | 0.00 | 0.08 | 16 | 37 |
| 18 | 4 31 36.9 | 17 42 34 | 4 | 15 | 60 | 20.8 | −0.14 | 0.05 | 0.01 | 0.08 | 11 | 12 |
| 19 | 4 31 40.0 | 18 13 54 | 4 | 17 | 20 | 10.0 | 0.97 | 0.04 | −0.01 | 0.09 | 17 | 11 |
| 20 | 4 31 43.6 | 17 47 28 | 4 | 11 | 5.7 | 4.9 | 0.99 | 0.13 | 0.62 | 0.14 | ... | ... |
| 21 | 4 31 56.9 | 17 31 51 | 60 | 27 | 12 | 3.9 | ... | ... | ... | ... | ... | ... |
| 22 | 4 32 03.5 | 18 21 02 | 30 | 25 | 54 | 6.9 | 0.76 | 0.08 | 0.26 | 0.08 | 8 | 77 |
| 23 | 4 32 07.3 | 17 38 41 | 60 | 22 | 6.0 | 3.6 | ... | ... | ... | ... | ... | ... |
| 24 | 4 32 09.3 | 17 57 25 | 4 | 11 | 47 | 17.7 | 0.87 | 0.03 | 0.05 | 0.06 | 15–18 | 20 |
| 25 | 4 32 14.9 | 18 20 13 | 30 | 26 | 67 | 18.5 | 0.80 | 0.04 | 0.13 | 0.05 | 21–43 | 25 |
| 26 | 4 32 15.8 | 18 01 39 | 4 | 13 | 103 | 26.5 | 0.90 | 0.02 | 0.14 | 0.04 | 36–42 | 15 |
| 27 | 4 32 23.4 | 17 45 04 | 4 | 19 | 34 | 13.2 | −0.29 | 0.07 | 0.19 | 0.12 | 8 | 8 |
| 28 | 4 32 27.5 | 17 32 01 | 60 | 30 | 12 | 5.1 | ... | ... | ... | ... | ... | ... |
| 29 | 4 32 28.2 | 18 18 11 | 30 | 26 | 8.6 | 4.8 | ... | ... | ... | ... | ... | ... |
| 30 | 4 32 29.6 | 17 24 11 | 60 | 37 | 19 | 6.9 | ... | ... | ... | ... | ... | ... |
| 31 | 4 32 29.2 | 17 54 21 | 4 | 16 | 13 | 9.8 | −0.05 | 0.11 | 0.04 | 0.15 | ... | ... |
| 32 | 4 32 43.7 | 18 02 58 | 4 | 20 | 25 | 9.7 | 0.91 | 0.05 | 0.29 | 0.09 | 11–16 | 17 |
| 33 | 4 32 53.1 | 17 35 32 | 60 | 31 | 13 | 4.2 | ... | ... | ... | ... | ... | ... |
| 34 | 4 33 35.2 | 17 49 41 | 60 | 32 | 10 | 4.2 | ... | ... | ... | ... | ... | ... |
| 35 | 4 33 33.7 | 18 00 56 | 30 | 31 | 317 | 37.9 | 0.91 | 0.02 | 0.27 | 0.03 | 97–130 | 19 |
| 36 | 4 33 44.2 | 18 09 11 | 60 | 35 | 9.9 | 3.9 | ... | ... | ... | ... | ... | ... |
| 37 | 4 34 35.5 | 18 02 06 | 60 | 46 | 43 | 3.8 | 1.00 | 0.20 | 0.55 | 0.09 | 39–40 | 50 |
| 38 | 4 34 40.8 | 17 44 46 | 60 | 49 | 28 | 3.7 | ... | ... | ... | ... | ... | ... |

each of which feeds a separate detector (Tanaka, Inoue, & Holt 1994). Two detectors are gas scintillation proportional counters (Gas Imaging Spectrometer, or GIS), and two are CCD detectors (Solid-state Imaging Spectrometer, or SIS). The SIS has better energy resolution than the GIS, while the GIS has a wider field of view. The fields of view of both detector systems are considerably narrower than that of the *ROSAT* PSPC, as shown in Figure 1.

*ASCA* pointed at the L1551 cloud for about 90,000 s continuously on 1994 February 23 and 24. Good data were extracted from the telemetry stream with the clean_sis and clean_gis routines in the XANADU software reduction system provided by the High Energy Astrophysics Science Archive Research Center (HEASARC). In addition to the usual removal of periods of Earth blockage and South Atlantic Anomaly passage, we rejected data taken while the satellite was pointed near the bright terrestrial atmosphere ($<25°$ from the bright Earth and $<10°$ from the dark Earth) and during periods of high particle background flux. Hot and flickering pixels were removed from the SIS data, which were obtained in the bright 4-CCD mode. After these screening operations, the useful exposure times were about 40,000 s for the GIS and 33,000 s for the SIS detectors.

Within the 50′ diameter circular field of the GIS, seven sources are clearly seen (Fig. 3). The additional "source" at

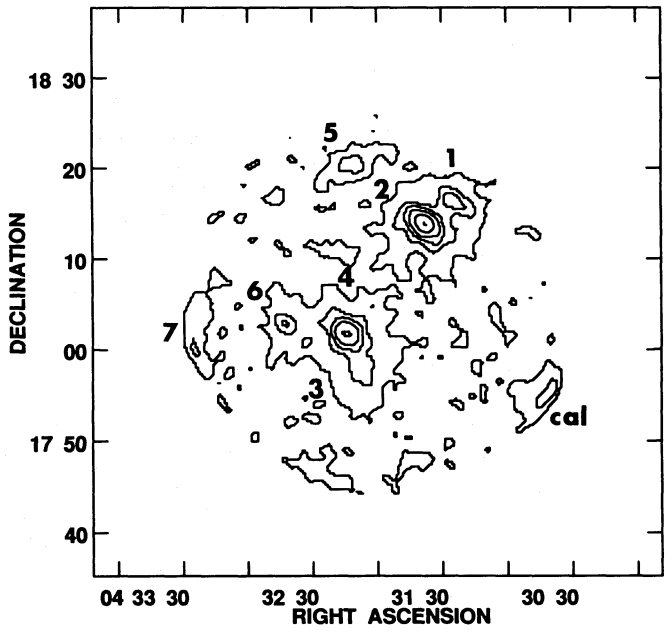


FIG. 3.—Contour map of the *ASCA* GIS field, showing surface densities of 1, 2, 3, 4, 5, 6, 8, 12, and 25 events $pixel^{-1}$. Sources are labeled as indicated in Table 2.

TABLE 2

*ASCA* SOURCES NEAR THE L1551 CLOUD

| *ASCA* SOURCE | L1551X SOURCE | R.A. (2000) | DECL. (2000) | *ASCA-ROSAT* OFFSET | COUNT RATES ($ks^{-1}$) | | | |
|---|---|---|---|---|---|---|---|---|
| | | | | | GIS2 | SIS0 | *ROSAT* | *Einstein* IPC |
| 1 ..... | 14 | $4^h31^m26^s$ | 18°16'37" | 23 | 11 | ... | 151 | 45 |
| 2 ..... | 19 | 4 31 40 | 18 14 13 | 19 | 29 | 60 | 20 | 17 |
| 3 ..... | 24 | 4 32 07 | 17 56 49 | 50 | 8 | 12 | 47 | 15–18 |
| 4 ..... | 26 | 4 32 15 | 18 01 37 | 12 | 22 | 47 | 103 | 36–42 |
| 5 ..... | 25 | 4 32 17 | 18 20 28 | 35 | 5 | ... | 67 | 21–43 |
| 6 ..... | 32 | 4 32 43 | 18 02 56 | 11 | 6 | 10 | 25 | 11–16 |
| 7 ..... | 35 | 4 33 33 | 18 01 18 | 25 | 23 | ... | 317 | 97–130 |

the southwest corner of the field is an on-board radioactive calibration source. These sources are listed in Table 2, with centroid locations determined by the *ASCA* aspect system without further correction. Despite the broad point-spread function of the *ASCA* mirror assemblies, the sources can be identified with *ROSAT* sources with offsets typically $<30''$. Only four of these sources lie within the smaller fields of view of the SIS detectors. Background for each detector was estimated from a large source-free region of the field and was removed from the source region. Table 2 gives the resulting background-subtracted count rates in the GIS2 and SIS0 detectors in the 0.1–10.0 keV band, along with *ROSAT* and *Einstein* count rates for comparison. Note that the conversions between count rates and fluxes are uncertain and may differ between sources and epochs. However, long-term variability can be seen; Source 2, for example, was the brightest source in the *ASCA* observation but was much fainter during the *ROSAT* and *Einstein* observations.

### 2.3. *Optical Observations*

Optical counterparts of the L1551 X-ray sources were found by inspection of the digitized Palomar Sky Survey, supplemented with cataloged stars listed in the SIMBAD database, the Hubble Space Telescope Guide Star Catalog (GSC), and the Herbig and Bell Catalog (HBC; Herbig & Bell 1988). Figure 4 (Plates 9–10) shows $2' \times 2'$ finding charts from the Sky Survey centered on the 38 boresight-corrected *ROSAT* locations. They were produced with the Guide Star Selection System Astronomic Support Program (GASP), developed by the Space Telescope Science Institute. Examination shows that in many cases the identification is obvious, with a single star clearly centered in the field, while in other cases multiple counterparts or no bright stars lie within the error circle.

Optical spectra of 15 of the previously unstudied stellar counterparts were obtained by one of us (I. N. R.) using the Palomar 1.5 m telescope. The observations were made under photometric conditions on 1993 December 27/28 using a 600 line $mm^{-1}$ grating to give a dispersion of 1.5 Å $pixel^{-1}$, a resolution of $\sim$3.5 Å, and wavelength coverage from 6200 to 7400 Å. The data were bias-subtracted, flat-fielded, and extracted using standard techniques and were calibrated to a flux scale with observations of standard stars from Oke & Gunn (1983). The spectra, with typical S/N $\simeq$ 50, were searched for H$\alpha$ emission and Li 6707 Å absorption characteristic of WTT stars.

Proper motions were determined via Palomar Sky Survey Plates taken with the Oshin 48 inch (1.2 m) Schmidt Telescope and with plates taken with the UK Schmidt Telescope (UKST). The plates were scanned by the COSMOS plate measuring engine at the Royal Observatory, Edinburgh (MacGillivray & Stobie 1984). Methods of data reduction and analysis are given in Reid (1990, 1992). Each plate covers $\sim 5\overset{\circ}{.}3 \times 5\overset{\circ}{.}3$. Spurious sources are eliminated by comparing plates from the same epoch and only considering those sources which appear on both. Proper motions are determined from offsets between source positions on plates of different epochs.

## 3. STELLAR IDENTIFICATIONS

Table 3 lists likely optical counterparts of the *ROSAT* sources along with their offset from the X-ray position and *V* magnitude. The classifications in columns (3) and (4) follow those used by FCMG in the Chamaeleon cloud. Column (3) gives our suggested classification of the optical counterpart: CTT star (C), WTT star (W), potential "new" T Tauri stars with $10 \leq V \leq 16$ (N or N?), the early-type pre–main-sequence star HD 28867 (B9), and sources "unrelated" to the cloud (U). Column (4) gives our evaluation of the reliability of the proposed stellar identification. Reliability Class 1 indicates that a single star or unresolved binary lies in a small *ROSAT* error circle; Class 2 indicates that two or more stellar counterparts are plausible, often because the X-ray source has a large error circle; and Class 3 indicates that the field has many possible counterparts or the reality of the X-ray source is suspect. When a *ROSAT* error circle contains more than one prominent star, each is listed in order of proximity to the X-ray centroid. We consider each class of stellar identification in more detail.

### 3.1. *Known Cloud Members*

Considering the known T Tauri population of the cloud that lie in the *ROSAT* field of view (Herbig & Bell 1988; see Fig. 1), one to three of the six CTT stars and five to seven of the eight known WTT stars are detected. Of the CTT stars XZ and V710 Tau A are detected, GG Tau is possibly detected, and HL, HN, and DM Tau are not detected. Of the WTT stars, UX Tau (A or B), L1551-51, V827 Tau, V826 Tau, and L1551-55 are detected, while HBC 392 and V710 Tau B are possibly detected. The sample of detected T Tauri stars is too small to correlate independently X-ray emission with stellar properties, but it can be compared to other surveys. Assuming a distance of 140 pc, approximate X-ray luminosities can be estimated from the count rates with the average relation 1 count $ks^{-1} \simeq 3 \times 10^{28}$ ergs $s^{-1}$ (FCMG), which is consistent with luminosities obtained from spectral model fits (§ 4.1). Determination of the stellar properties of the X-ray sources is complicated by the fact that at least five of the 12 cloud members are binary stars (UX Tau, XZ Tau, V710 Tau, L1551-51, and V826 Tau). In

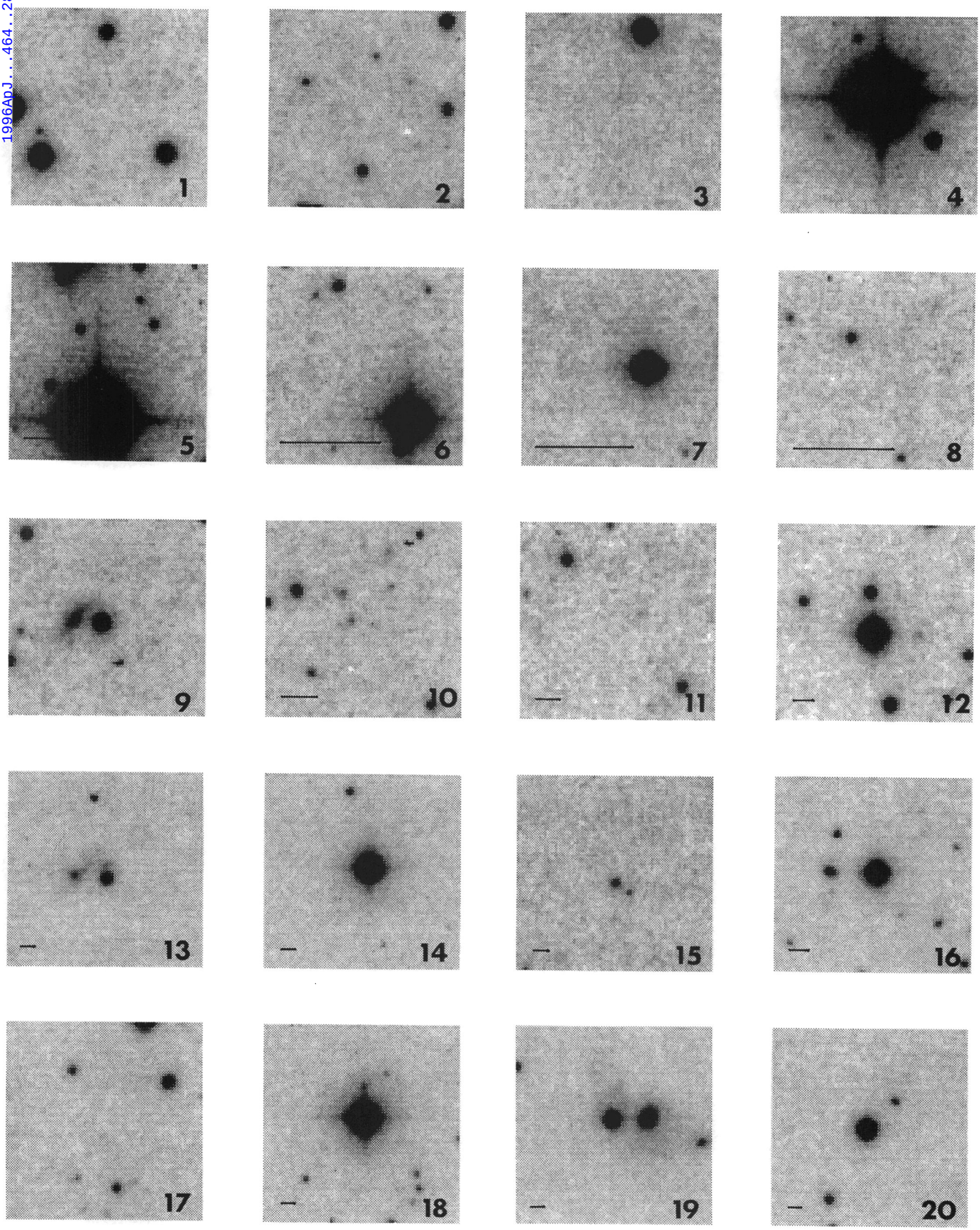


FIG. 4.—Finding charts for L1551X 1–38, produced with the STScI GASP database. Each picture is 2′ by 2′, and the line represents the diameter of the 90% error circle. Charts without lines have error circles 2′ in diameter.

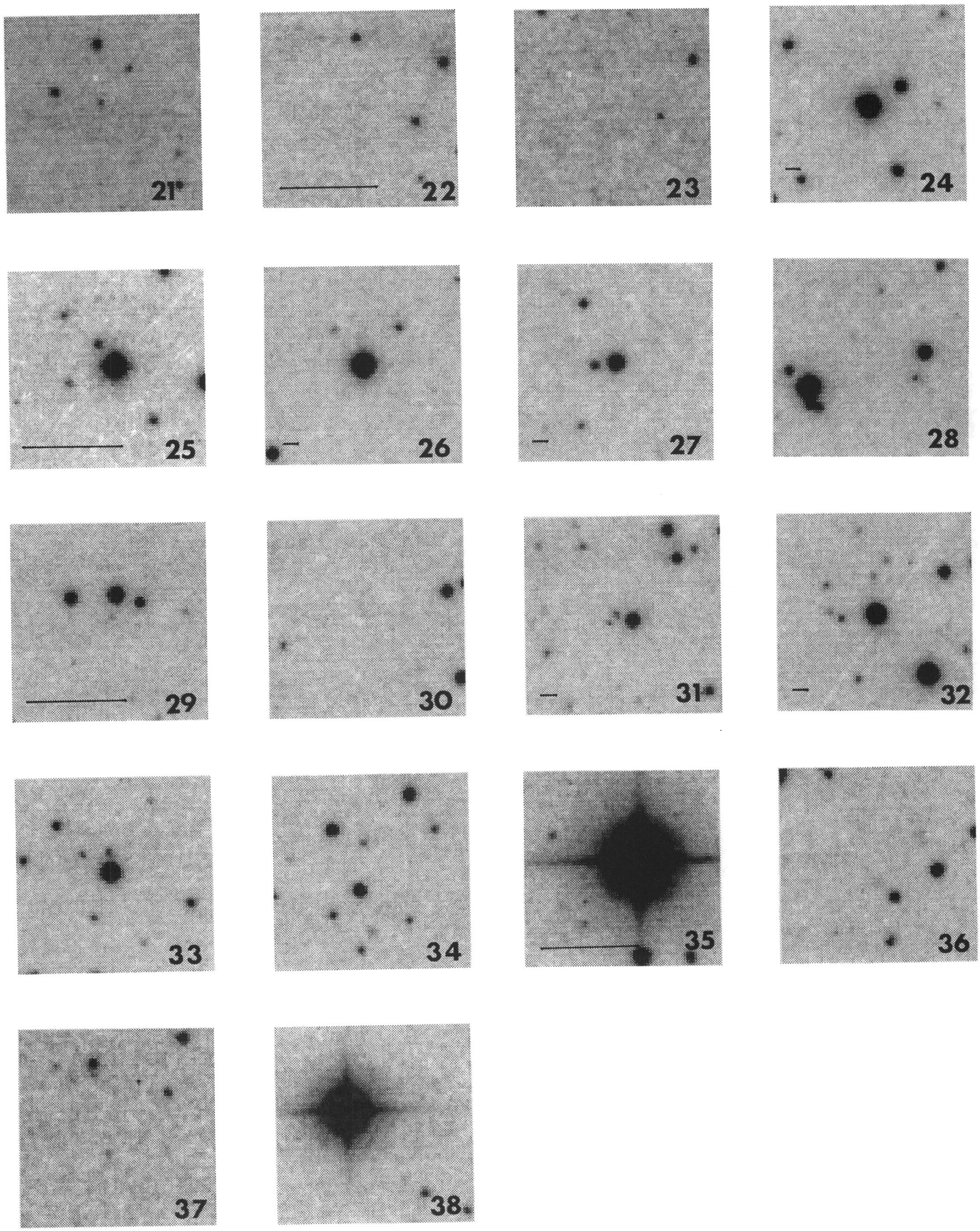


FIG. 4—*Continued*

TABLE 3

STELLAR IDENTIFICATIONS

| L1551X Source (1) | *ASCA* Source (2) | Class (3) | Reliability (4) | Offset (5) | $V$ (6) | GSC (7) | HBC (8) | Other Name (9) |
|---|---|---|---|---|---|---|---|---|
| 1 ..... | ... | U | 2 | 47″ | 13.3[a] | 1269_989 | ... | ... |
| | ... | U | 2 | 54 | 11.8[a] | 1269_1208 | ... | ... |
| | ... | U | 2 | 61 | 11.8[a] | 1269_957 | ... | ... |
| | ... | U | 2 | 130 | 12.2[b] | 1269_1045 | ... | vA 486 (Hyad) |
| 2 ..... | ... | U | 2 | 100 | 7.8[b] | ... | ... | vB 73 (Hyad) |
| 3 ..... | ... | U | 1 | 52 | 11.7[a] | 1269_543 | ... | ... |
| 4 ..... | ... | U | 1 | 8 | 7.1[b] | 1269_294 | ... | vB 77 (Hyad) |
| 5 ..... | ... | U | 1 | 38 | 6.9[b] | 1269_557 | ... | vB 78 (Hyad) |
| 6 ..... | ... | U | 1 | 47 | 9.8[b] | ... | ... | vB 79 (Hyad) |
| 7 ..... | ... | W | 1 | 18 | 10.7[c] | 1269_225 | 43 | UX Tau A |
| | ... | W | 1 | 23 | 13.7[c] | ... | 42 | UX Tau B |
| 8 ..... | ... | N? | 1 | 24 | 16[d] | ... | ... | ... |
| 9 ..... | ... | U | 2 | 8 | 14.0[b] | 1269_232 | ... | LP 415-418 (Hyad) |
| 10 ..... | ... | U | 3 | ... | 19:[d] | ... | ... | ... |
| 11 ..... | ... | U | 3 | ... | >19[d] | ... | ... | ... |
| 12 ..... | ... | U | 1 | 8 | 10.9[a] | 1269_693 | ... | L1551-26 |
| 13 ..... | ... | U | 1 | 7 | 15.0[b] | ... | ... | LP 415-1165 |
| 14 ..... | 1 | U | 1 | 8 | 10.4[b] | 1269_469 | ... | HD 285845 |
| 15 ..... | ... | N | 1 | 11 | 16[d] | ... | ... | ... |
| 16 ..... | ... | U | 1 | 1 | 11.9[b] | 1269_867 | ... | Lei 69 (Hyad) |
| 17 ..... | ... | U | 2 | 53 | 14.7[c] | 1269_218 | ... | ... |
| | ... | W | 2 | 69 | 12.5[c] | ... | 392 | ... |
| 18 ..... | ... | U | 1 | 4 | 10.4[b] | ... | ... | Lei 63 (Hyad) |
| 19 ..... | 2 | C | 1 | 3 | 13.3[c] | 1269_171 | 50 | XZ Tau |
| 20 ..... | ... | N? | 1 | 4 | 12.5[a] | 1269_771 | ... | L1551-35 |
| 21 ..... | ... | U | 2 | 16 | ... | ... | ... | 87GB 042903.5+172452 |
| 22 ..... | ... | C | 2 | 93 | 13.6[c] | ... | 51 | V710 Tau A |
| | ... | W | 2 | 93 | 14.6[c] | ... | 395 | V710 Tau B |
| 23 ..... | ... | U | 2 | 71 | 15.3[b] | ... | ... | LP 415-187 (Hyad) |
| 24 ..... | 3 | W | 1 | 2 | 12.1[c] | 1270_1195 | 397 | L1551-51 |
| 25 ..... | 5 | W | 1 | 6 | 12.2[c] | 1270_1108 | 399 | V827 Tau |
| 26 ..... | 4 | W | 1 | 0 | 12.1[c] | ... | 400 | V826 Tau |
| 27 ..... | ... | U | 1 | 2 | 13.8[a] | 1270_507 | ... | HZ 9 (Hyad) |
| 28 ..... | ... | N? | 2 | 26 | 14.5[a] | 1270_1313 | ... | ... |
| | ... | C | 2 | 51 | 12.2[c] | 1270_897 | 54 | GG Tau |
| 29 ..... | ... | N? | 1 | 17 | 13.9[a] | 1270_403 | ... | ... |
| 30 ..... | ... | ... | 3 | ... | ... | ... | ... | ... |
| 31 ..... | ... | U | 1 | 8 | 15[d] | ... | ... | vA 674 (Hyad) |
| 32 ..... | 6 | W | 1 | 2 | 13.2[c] | 1270_958 | 403 | L1551-55 |
| 33 ..... | ... | N | 1 | 2 | 13.3[a] | 1270_735 | ... | ... |
| 34 ..... | ... | N? | 2 | 56 | 15.2[a] | 1270_922 | ... | ... |
| 35 ..... | 7 | B9 | 1 | 13 | 6.3[b] | ... | ... | HD 28867 |
| 36 ..... | ... | ... | 3 | ... | ... | ... | ... | ... |
| 37 ..... | ... | ... | 3 | ... | ... | ... | ... | ... |
| 38 ..... | ... | U | 1 | 20 | 8.0[b] | 1270_806 | ... | SAO 94015 |

[a] Guide Star Catalog.
[b] SIMBAD database.
[c] Herbig-Bell catalog 1988.
[d] Visual inspection of digitized Palomar Sky Survey

these cases, the brightest star is assumed to be the X-ray source, which is justified by the correlation of increasing $L_X$ with $L_{bol}$ (FCMG). Stellar properties are obtained from information in Herbig & Bell (1988), Walter et al. (1988), and Hartigan, Strom, & Strom (1994).

A comparison of the X-ray luminosities and V magnitudes for the L1551 T Tauri stars matches well the linear relationship found for the Chamaeleon I cloud in FCMG, if an offset is allowed to take into account that FCMG use $R$ instead of $V$ magnitudes ($V-R \sim 1$). At 140 pc, the L1551 members have roughly the same distance modulus as the members of Chamaeleon I. The X-ray luminosity function for the L1551 T Tauri stars is roughly consistent with that found in the Chamaeleon I cloud (FCMG). Most of the detected sources are WTT stars with $\log L_X \sim 30$. No correlation is found between X-ray luminosity and surface rotation velocity, $v \sin i$, for nine stars with measured rotation. Note that stellar dynamo model of magnetic field generation predicts such a correlation, which was also missing in the Chamaeleon data (FCMG; Pallavicini et al. 1981.)

### 3.2. *Sources Unrelated to the Cloud*

Ten or 11 of the 21 *ROSAT* sources are produced by Hyads (Table 3). These identifications are based on the Hyades membership catalog of Reid (1993). Three sources are foreground objects. Source 13 is LP 415-1165, a foreground dM star appearing in the Luyten (1971) proper-motion catalog. It is projected onto the L1551 IRS 5 bipolar flow in the middle of the cloud (Cudworth & Herbig 1979). Source 14, HD 285845, is a binary system excluded from cloud membership by its radial velocity (Walter et al. 1988) and proper motion. Source 38 is a $V = 8$ main-sequence F3

star in front of the cloud (Kenyon et al. 1994); bright F stars such as this are common serendipitous sources in soft X-ray images (Feigelson et al. 1987). Five "U" sources are rejected as possible new T Tauri stars in § 3.3, but we have no firm indication of their status. These objects may be foreground dwarfs, background active stars, or unrelated to the true X-ray source.

Three "U" sources in Table 3 are likely to be extragalactic: L1551X 10, 11, and 21. It is reasonable to expect several extragalactic sources in the *ROSAT* regions outside the obscuring cloud, where the Galactic column density is relatively transparent at $1\text{–}2 \times 10^{21}$ cm$^{-2}$ (Stark et al. 1992). Extragalactic soft X-ray sources with fluxes of order $10^{-13}$ ergs s$^{-1}$ cm$^{-2}$ typically have quasar counterparts around $18 < V < 22$. The position of source 21 matches a 0.4 Jy (1.4 GHz) radio source with no counterpart on the Palomar Survey. It is likely to be a radio-loud quasar. Source 11 similarly has no Palomar Survey counterpart and may be a radio-quiet quasar. The finding chart of source 10 shows a group of faint galaxies. The object nearest to the X-ray centroid has $B-V = 0.80$, consistent with a normal galaxy.

### 3.3. *Possible New T Tauri Stars*

There are 14 *ROSAT* sources associated with stars that are neither known cloud members nor clearly unrelated to the cloud. Any of these must be considered to be a possible new WTT star. Seven have Reliability Class 1, four have Reliability Class 2, and three are unreliable identifications. Nine are in the Guide Star Catalog, while five are fainter and appear only on the digitized Palomar Survey. The Reliability 1 stars typically are among the faintest X-ray sources in the field.

Three methods are used in order to classify the potential new T Tauri stars. First, optical spectroscopy has been obtained for a few of the proposed new cloud members. Two were observed at low resolution in the survey for weak-Hα stars by Feigelson & Kriss (1983), and seven were observed by us to search for Hα emission and Lithium absorption features. Second, we have determined proper motion for most of the stellar counterparts of the *ROSAT* sources. The confirmed cloud members from the HBC, discarding those objects that may have their proper motions confused by nebulosity, have a mean of $\mu_\alpha = 0\farcs009$ yr$^{-1}$ and $\mu_\delta = -0\farcs019$ yr$^{-1}$ (see also Cudworth & Herbig 1979, Jones & Herbig 1979, and Gomez et al. 1992.) Third, we can examine whether the star's ratio of X-ray to optical brightness is consistent with the locus of confirmed *ROSAT*-detected WTT stars in the Chamaeleon cloud (FCMG; Huenemoerder, Lawson, & Feigelson 1995), which range from $\log L_X \simeq 29.7$ ergs s$^{-1}$ at $R = 12$ to 29.0 ergs s$^{-1}$ at $R = 16$.

Table 4 summarizes these findings for 16 stars associated with the 14 *ROSAT* sources that may be possible new T Tauri stars. L1551X number, Guide Star Catalog number, reliability class, and information on spectroscopy, proper motion, and position on X-ray/optical brightness diagram are given. Under the spectroscopy column a "Yes" indicates the presence of a feature, a "No" indicates its absence, and a "?" indicates that the S/N was too low to make a determination. Under the third heading of the proper-motion column is our evaluation of the proper motions of the stars compared to known cloud members. A "Yes" indicates proper motion within $\sim 0\farcs01$ yr$^{-1}$ of the cloud mean, a "Yes?" indicates sources within $\sim 0\farcs02$ yr$^{-1}$ of the mean, and a "No" indicates sources $\geq 0\farcs02$ yr$^{-1}$ from the mean. Under the "X-ray/optical" column a "Yes" indicates sources that fall within the locus of points that contain the T Tauri stars in Figure 10*a* of FCMG. The last column gives our identification as unrelated (U), likely new T Tauri star (N), or possible new T Tauri star (N?). No data are available for possible counterparts to the reliability class 3 sources L1551X 30, 36, and 37, so classifications are omitted for these sources. Remarks on individual sources follow.

*L1551X 1.*—This source is far off axis and has a large error circle containing three GSC sources. None of the stars fall in the region of the X-ray optical brightness diagram populated by T Tauri stars, none show Hα or Li 6707 Å features, and the proper motion is not within the range of known cloud members. It is unlikely that any of these stars is a T Tauri star. The Hyad vA 486 is a possible counterpart, but it is over 2′ from the X-ray centroid.

*L1551X 3.*—This object has neither Hα emission nor Li 6707 Å absorption and has proper motion inconsistent with

TABLE 4

PROPERTIES OF POSSIBLE "NEW" T TAURI STARS

| L1551X | GSC | Reliability Class | Spectroscopy | | Proper Motion | | | $f_X/f_O$ Relation | Class |
|---|---|---|---|---|---|---|---|---|---|
| | | | Hα? | Li ? | μ (arcsec yr$^{-1}$) | δ (arcsec yr$^{-1}$) | Member? | | |
| 1 ..... | 1269_989 | 2 | No | No | 0.014 | −0.003 | No | No | U |
| 1 ..... | 1269_1208 | 2 | No | No | 0.001 | −0.008 | No | No | U |
| 1 ..... | 1269_957 | 2 | No | No | −0.003 | 0.005 | No | No | U |
| 3 ..... | 1269_543 | 1 | No | No | −0.006 | −0.021 | No | Yes | U |
| 8 ..... | ... | 1 | ... | ... | ... | ... | ... | No | N? |
| 12 ..... | 1269_693 | 1 | No | No | −0.046 | 0.017 | No | No | U |
| 15 ..... | ... | 1 | ... | ... | 0.014 | −0.017 | Yes | Yes | N |
| 17 ..... | 1269_218 | 2 | No | ? | −0.004 | −0.001 | No | No | U |
| 20 ..... | 1269_771 | 1 | Yes | No | 0.008 | −0.002 | Yes? | Yes | N? |
| 28 ..... | 1270_1313 | 2 | ... | ... | 0.025 | −0.019 | Yes? | Yes | N? |
| 29 ..... | 1270_403 | 1 | No | ? | −0.004 | −0.019 | Yes? | Yes | N? |
| 30 ..... | ... | 3 | ... | ... | ... | ... | ... | ... | ... |
| 33 ..... | 1270_735 | 1 | Yes | Yes | 0.008 | −0.018 | Yes | Yes | N |
| 34 ..... | 1270_922 | 2 | ... | ... | 0.000 | −0.007 | Yes? | Yes | N? |
| 36 ..... | ... | 3 | ... | ... | ... | ... | ... | ... | ... |
| 37 ..... | ... | 3 | ... | ... | ... | ... | ... | ... | ... |

cloud membership, although its optical brightness and X-ray emission are consistent with T Tauri status. L1551X 3 is probably unrelated to the cloud.

*L1551X 8.*—This is a $V \sim 16$ mag uncataloged star with no spectral or proper-motion information. It seems to be overluminous in X-rays for its optical magnitude, but with no other information it has been classified as a possible new T Tauri star.

*L1551X 12.*—This GSC star corresponds to source L1551-26 in Feigelson & Kriss (1983). It is a $V = 10.9$ G5 star with $A_V = 1.7$ and no Hα emission. Its bright magnitude, heavy reddening, low X-ray luminosity, and absent Hα are inconsistent with a WTT identification. Its proper motion is far from the mean of cloud members. We suspect it is a background G giant.

*L1551X 15.*—This is a faint, very red star ($V = 18.4$ and $B-V = 2.4$), with proper motion consistent with cloud membership. This is a probable deeply embedded T Tauri star.

*L1551X 17.*—This GSC star is overluminous in X-rays for its optical brightness, has no Hα or lithium features in its spectrum (although the signal to noise is low), and has proper motion inconsistent with cloud membership. This X-ray source may instead be associated with the WTT star HBC 392. Although it is outside the *ROSAT* error circle, L1551X 17 is at the very edge of the *ROSAT* field, and its position may well be inaccurate. However, it has a soft excess, rarely seen in WTT stars (§ 4.1).

*L1551X 20.*—This corresponds to L1551-35 in Feigelson & Kriss (1983), who find $V = 12.5$, G8 spectral type, $A_V = 1.6$, and EW(Hα) = 0.6 Å. Feigelson and Kriss consider it to be a likely WTT star. It falls among the T Tauri stars in the X-ray/optical brightness diagram. Its proper motion is $\mu_\alpha = 0''.008$ yr$^{-1}$, $\mu_\delta = -0''.002$ yr$^{-1}$, which is about $0''.02$ yr$^{-1}$ from the mean for cloud members. If it is at a distance of 140 pc, its $L_{\rm bol} = 0.8\ L_\odot$ and lies on or close to the ZAMS, making it older than all other T Tauri stars associated with the cloud. L1551X 20 may thus be one of the handful of X-ray–discovered "post–T Tauri" stars or older Cas-Tau association members found in the Taurus-Auriga complex (Walter et al. 1988; Hartmann et al. 1991). We classify it as a possible new cloud member.

*L1551X 28.*—This is a GSC star for which we have no spectral information. It falls among the T Tauri stars in the X-ray/optical brightness diagram and has proper motion reasonably near the mean of known cloud members. While the GSC star is a possible new T Tauri star, it is also possible that the source is the CTT star GG Tau $51''$ from the source centroid. We classify this star as "N?."

*L1551X 29.*—This star has no Hα emission or Li 6707 Å absorption in its spectrum (although the S/N is low). However, it falls among the T Tauri stars in the X-ray/optical brightness diagram and has proper motion not inconsistent with the cloud. We classify it as "N?."

*L1551X 30.*—The field around this source has several GSC stars, none of which are closer than $50''$ from the source. We can make no clear identification for this source, but it is possible that it is a T Tauri star.

*L1551X 33.*—This GSC star is has an M spectral type with EW(Hα) = 2.7 Å, $V = 13.8$, and $B-V = 1.6$. It has proper motion $\mu_\alpha = 0''.008$ yr$^{-1}$ and $\mu_\delta = -0''.018$ yr$^{-1}$, placing it very close to the mean of cloud members. It also has a location on the X-ray/optical brightness diagram near the locus for T Tauri stars. This is very likely a new WTT star.

*L1551X 34.*—This GSC star has a location on the X-ray/optical brightness diagram within the region populated by T Tauri stars, has a proper motion reasonably near the mean of known cloud members, and has no available spectra. Although it is the closest star to the X-ray centroid, the identification is not strong because there are other stars in the error circle.

*L1551X 36.*—As with L1551X 30, there is no clear identification for this source.

*L1551X 37.*—This source also has no clear identification.

In addition to determining cloud membership, proper motion can also be used to determine if any of these objects are members of the Hyades. None of the objects have proper motions near the mean of the Hyades ($\mu_\alpha = 0''.110$ yr$^{-1}$, $\mu_\delta = -0''.030$ yr$^{-1}$.) Thus it is unlikely that any of these sources are Hyades members. In summary, of the 14 *ROSAT* sources possibly produced by new Tauri stars, two are likely new WTT stars (L1551X 15 and 33), five are possible new cloud members, four are unrelated to the cloud, and for three we can make no determination.

### 3.4. *Embedded Protostars and Ejecta*

None of the three embedded *IRAS* sources, including L1551 IRS 5 and L1551NE that power the powerful bipolar flow and HH 28/29 complex, are detected in either the *ROSAT* or *ASCA* images. Similarly, neither the L1551 IRS 5 flow itself nor any of the Herbig-Haro objects are seen. X-ray emission from high-temperature shocks associated with Herbig-Haro objects has been speculated, but there have been no confirmed reports of its detection (Pravdo & Marshall 1981). Of the seven HH objects in Figure 1 (HH 28, 265, 102, 29, 30, 266, 262), none are detected by *ROSAT* down to a level of 2 counts ks$^{-1}$. *ROSAT* source 13 appears in the western lobe of the flow but is a pointlike soft source that is readily identifiable with a foreground dM star. There is thus no evidence for X-ray emission from either the embedded protostars or their ejecta.

The upper limits to their luminosities depend on the assumed absorption to the emitting surface. The most stringent limit can be obtained for L1551 IRS 5, which lies near the center of the *ASCA* field and, if X-ray–emitting, would be well resolved from other X-ray stars. It was not detected with a 3 $\sigma$ limit of 3.0 counts ks$^{-1}$ in the 0.5–10 keV band. Assuming an intrinsic spectrum similar to that seen in the X-ray–bright T Tauri stars (§ 4.2 below), this corresponds to luminosity limits of $1.5 \times 10^{29}$ ergs s$^{-1}$ for $N_{\rm H} = 1 \times 10^{21}$ cm$^{-2}$, $3.7 \times 10^{29}$ ergs s$^{-1}$ for $N_{\rm H} = 1 \times 10^{22}$ cm$^{-2}$, and $2.6 \times 10^{30}$ ergs s$^{-1}$ for $N_{\rm H} = 1 \times 10^{23}$ cm$^{-2}$. We note that Casanova et al. (1995) reports possible detections of several protostars at levels comparable to these limits. These detections are in the $\rho$ Ophiuchi core, where identification is greatly hindered by crowding.

### 3.5. *Summary*

We find that two to three of the 38 *ROSAT* sources are produced by CTT stars, five to seven by previously known WTT stars, two by new T Tauri stars, five by possible new T Tauri stars, one by the B9e star HD 28867, three by sources with no information to make a determination, and 21 by stars or extragalactic objects unrelated to the cloud. Twenty-four of these proposed identifications have Reliability Class 1 and are very likely to be correct. Counterpart ambiguities or uncertainties are present in the remaining 14 sources.

Each of the seven *ASCA* sources can be unambiguously matched to a prominent *ROSAT* source, as indicated in Table 3. Five are associated with well-known CTT or WTT stars, one is unrelated to the cloud, and one is produced by the B9 star HD 28867. Since the *ASCA* pointing was centered on the cloud, nearly all of the sources are cloud members.

## 4. X-RAY SPECTRAL ANALYSIS

### 4.1. *ROSAT Spectra*

Photons from each *ROSAT* source were extracted using IRAF/PROS software. Because of the deterioration of the point-spread function with off-axis distance, three extraction radii were used: 1.′75 for sources with $\theta \leq 20'$, 3′ for $20' < \theta < 30'$, and 5′ for $\theta > 30'$. Background subtraction was accomplished in two ways. For sources with $\theta < 20'$, the background spectrum was defined in a source-free region $\sim 8'$ across. For the outer areas where telescope vignetting and window support structure affect background levels, a local region around each source was used.

A simple model-independent measure of the X-ray spectrum is shown in Figure 5, a color-color plot of hardness ratios within the PSPC band, for the stronger PSPC sources. The hardness ratios are defined as HR 1 $= (B-A)/(B+A)$ and HR 2 $= (D-C)/(D+C)$, where $A$ is the number of counts from 0.11 to 0.42 keV, $B$ is the number of counts from 0.52 to 2.02 keV, $C$ is the number of counts from 0.52 to 0.91 keV, and $D$ is the number of counts from 0.91 to 2.02 keV. Hardness ratios are given in Table 1. A positive value of HR 1 indicates a source in which most of the counts are in the hard band, while a negative value indicates a source dominated by soft photons. High values of HR 1 ($\sim 1$) often indicate moderate extinction ($N_{\rm H} \simeq 10^{21}$ cm$^{-2}$), while increasing values of HR 2 are correlated with increasing temperature (Neuhäuser et al. 1995a).

Examination of Figure 5 reveals that all sources fall into two distinct regions: a hard group spanning HR 1 $\sim 0.75$ to 1.00, and a soft group spanning HR 1 $\sim -0.40$ to 0.0. The hard group contains heavily obscured objects which are mostly T Tauri stars. The soft group contains objects with low extinction, including Hyads and foreground stars. The distribution of HR 2 in the two groups is the same. This pattern suggests that T Tauri and foreground stars have similar intrinsic spectra, but soft components in T Tauri star spectra are absorbed along the line of sight. Neuhäuser et al. (1995a) finds a similar relation in data from the shallow *ROSAT* All-Sky Survey of the Taurus-Auriga region. There is no apparent difference between WTT and CTT stars on this diagram, although it only contains two CTT stars.

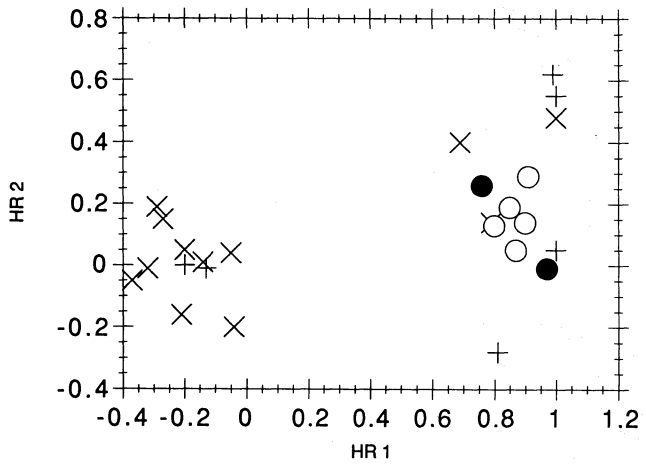


FIG. 5.—Plot of the *ROSAT* hardness ratios HR 1 vs. HR 2. The symbols define the object's classification from Table 3: WTT star (*open circles*), CTT star (*filled circles*), unrelated to the cloud (*crosses*), candidate "New" T Tauri star (*plus signs*).

Of the six possible new T Tauri stars for which we have hardness ratios, four sources (L1551X 12, 15, 20, and 37) have positive values of HR 1. Recall that sources 15 and 20 have spectroscopic properties and proper motions consistent with membership, whereas source 12 does not, and for source 37 we have little information on which to base our decision (§ 3.3). Source 12 is thought to be an absorbed background object, which would explain its position near the T Tauri stars. This indicates that hardness ratio diagrams should not be used by themselves to determine a star's status as a T Tauri star. Sources L1551X 1 and 17 have negative values of HR 1, which places them in the region containing foreground objects.

We initially approached spectral modeling using a solar analogy, where plasma with different temperatures can be present but always with solar elemental abundances. The Raymond-Smith plasma model with soft X-ray absorption based on Morrison-McCammon atomic cross sections is used throughout (Morrison & McCammon 1983.) Plasma models are fitted to the X-ray pulse height distributions using the XSPEC package (version 8.32). Pulse height data for the harder T Tauri stars generally show a peak at $\sim 1$ keV, with a sharp cutoff toward higher energies and a gradually sloping soft tail. The data for six of these sources are shown in the right-hand panels of Figure 6. The softer foreground stars show a similar peak around 1 keV plus a second peak around 0.2 keV.

Two-temperature models for the 12 *ROSAT* sources with sufficient counts for meaningful fitting are given in Table 5. The columns list the model parameters (plasma temperature $kT$, foreground column density $N_{\rm H}$, and normalization), energy range over which the fit was performed, extraction circle radius, total flux over the given energy range, and the percentage of the total flux contributed by the low temperature component (% Soft). Fits with acceptable values of $\chi^2$ require a two-temperature model in all but three sources. The components have temperatures around $kT_{\rm soft} \simeq 0.3$ keV and $kT_{\rm hard} \simeq 1.0$ keV, although these values are not well constrained.

### 4.2. *ASCA Spectra*

*ASCA* data analysis was based on *XANADU* software, using XSELECT (version 1.0) and XSPEC (version 8.50). Our analysis concentrates on the GIS2 proportional counter and the solid-state CCD SIS0 detector. The latter has a considerably higher spectral resolution, sufficient in principle to resolve individual emission lines. Seven sources, including six pre–main-sequence members of the L1551 cloud, are analyzed. Four sources—*ASCA* sources 2, 3, 4, and 6—are within the SIS field. The remaining three are analyzed using the GIS data. Source photons are extracted from circular regions with radii 1.′5–2.′5 for the SIS and 4.′0 and 4.′25 for the GIS. A background spectrum is subtracted from each source, obtained from the largest source-free region near the source (on the same CCD chip for SIS sources). Events are placed into 172 energy channels 0.07

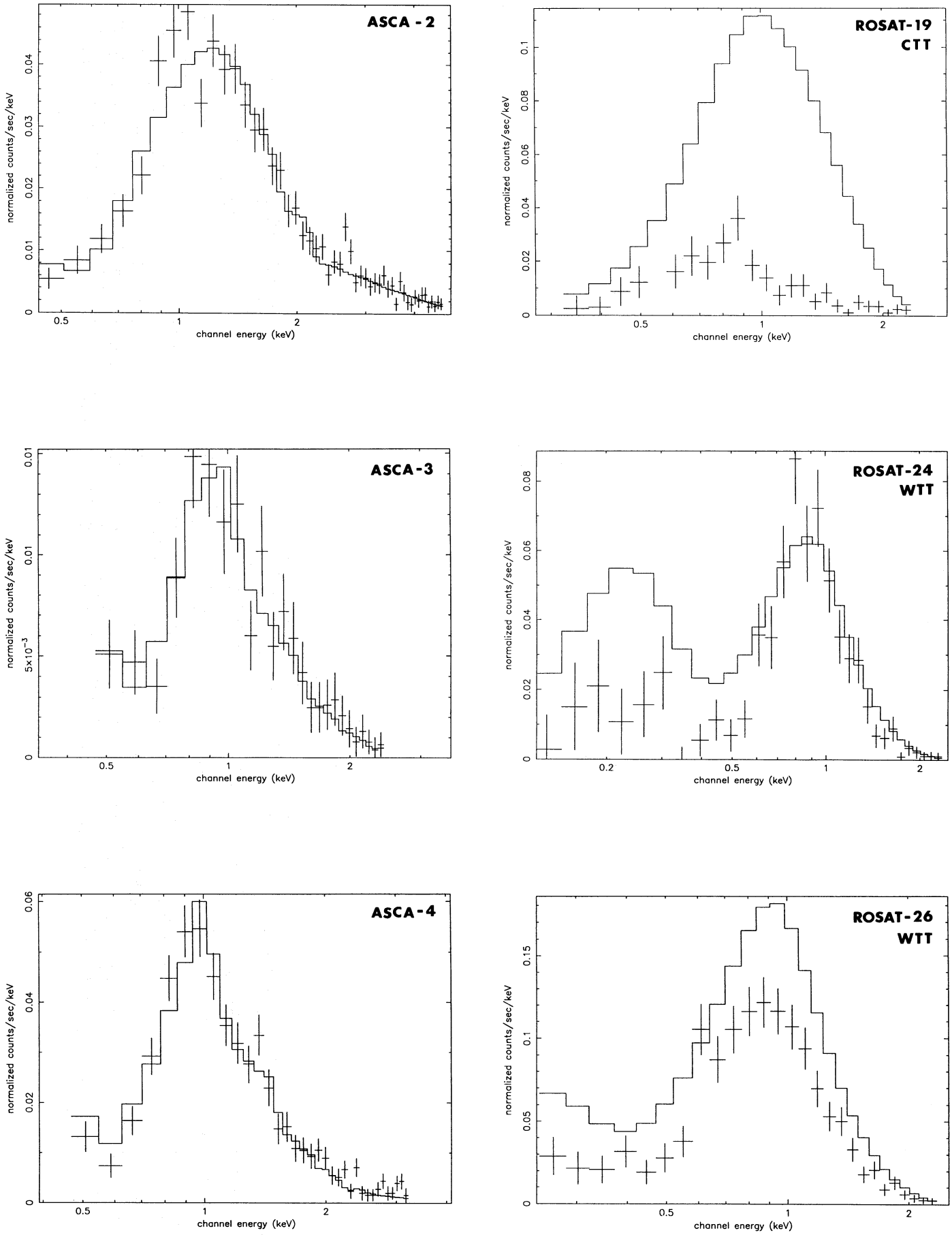


FIG. 6.—*Left-hand panels*: *ASCA* spectra of six sources with best fitting one-temperature, low abundance model from Table 6. *Right-hand panels*: *ROSAT* spectra of the same sources with the *ASCA* model.

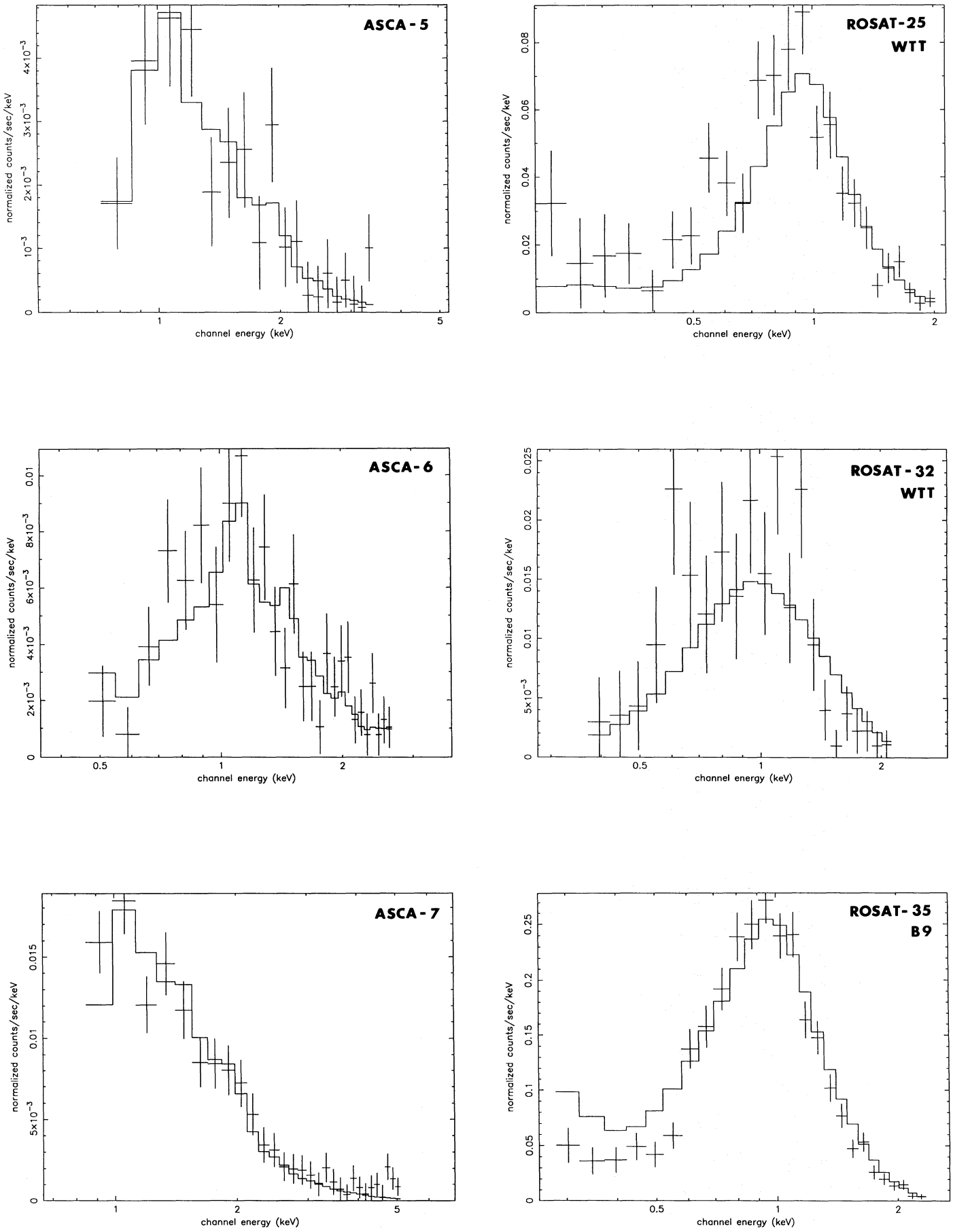


FIG. 6—*Continued*

TABLE 5

PARAMETERS FROM SPECTRAL FITS: *ROSAT*

| L1551X Source | Circle Size[a] | Energy (keV) | log $N_H$ ($cm^{-2}$) | $kT_1$ (keV) | $kT_2$ (keV) | $Norm_1$ ($10^{-18}$ $cm^{-5}$) | $Norm_2$ ($10^{-18}$ $cm^{-5}$) | $F_X$[b] | $\chi^2$ | % Soft |
|---|---|---|---|---|---|---|---|---|---|---|
| 1 ..... | c | 0.1–2.0 | 19.7 | 0.2 | 1.0 | 3.1 | 5.1 | 16.7 | 0.9 | 44 |
| 4 ..... | c | 0.1–1.6 | 19.3 | 0.1 | 0.6 | 2.1 | 2.7 | 12.4 | 1.2 | 37 |
| 5 ..... | b | 0.1–2.0 | 20.0 | 0.1 | 0.7 | 1.2 | 0.7 | 4.2 | 1.0 | ... |
| 7 ..... | b | 0.2–2.0 | 20.6 | ... | 1.0 | ... | 5.3 | 9.2 | 0.7 | ... |
| 9 ..... | b | 0.2–2.0 | 19.5 | 0.1 | 0.6 | 0.5 | 0.6 | 3.2 | 0.9 | 42 |
| 14 ..... | a | 0.1–2.0 | 20.6 | 0.2 | 1.1 | 2.3 | 7.0 | 15.7 | 1.1 | 34 |
| 18 ..... | a | 0.1–1.7 | 0 | 0.2 | 0.9 | 0.8 | 1.2 | 4.4 | 0.9 | 45 |
| 24 ..... | a | 0.1–2.0 | 20.5 | ... | 0.8 | ... | 2.1 | 5.3 | 0.9 | ... |
| 25 ..... | b | 0.2–2.0 | 20.8 | 0.2 | 1.0 | 2.0 | 4.5 | 13.0 | 1.1 | 37 |
| 26 ..... | b | 0.2–2.0 | 20.7 | 0.4 | 1.4 | 1.9 | 8.2 | 15.0 | 0.8 | 68 |
| 27 ..... | a | 0.1–1.6 | 19.9 | 0.1 | 0.9 | 0.6 | 0.6 | 2.3 | 0.9 | 50 |
| 35 ..... | b | 0.3–2.0 | 20.6 | ... | 1.1 | ... | 27.3 | 41.0 | 1.3 | ... |

[a] a = 1.'75; b = 3'; c = 5'.
[b] $F_X$ in units of $10^{-13}$ ergs $s^{-1}$ $cm^{-2}$.

keV wide for the SIS and 89 channels 0.14 keV wide for the GIS. The resulting spectra are shown in the left-hand panels of Figure 6. Note that the telescope-detector system is sensitive to X-rays up to $\simeq 10$ keV, but, except for two sources, no photons are seen above $\simeq 3$ keV. The exceptions are the CTT star XZ Tau (*ASCA* source 2) and the B9 star HD 28867 (*ASCA* source 7).

Following the *ROSAT* analysis, the data were modeled with a Raymond-Smith plasma model assuming cosmic abundances. A two-temperature plasma, with the standard cosmic ratios of elemental abundances, provides an adequate fit to five of the sources, but better fits with lower $\chi^2$ values are provided by plasma models with less-than-cosmic elemental abundances ($\lesssim 10\%$ of cosmic values.) Neither model can be discarded on the basis of $\chi^2$, and it is not clear which best represents the plasma properties. Low-abundance fits may indicate the inadequacy of the current plasma model or may arise from genuine abundance differences between stellar coronae and the accepted cosmic values.

The best-fitting parameters for both two-temperature and low-abundance models are given in Table 6 including extraction radius, detector, energy range over which the fit was performed, total flux over this band, and $\chi^2$. For those sources with available *ROSAT* spectra, $N_H$ values from the *ROSAT* fits are used, because of *ASCA*'s poor performance at low energies. For one-temperature low-abundance fits, the best temperature is generally $\sim 1$ keV. The exception is *ASCA* source 2 (XZ Tau) which is best fitted by a low-abundance plasma with temperature 2.3 keV. If a two-temperature model is used, the harder component has $3.2 \pm 1.1$ keV, comparable to the temperature seen by *Tenma* and *Ginga* in other star-forming clouds (Koyama 1987; Koyama et al. 1992). The best-fitting low-abundance model is superposed on the left-hand panels of Figure 6.

### 4.3. *ROSAT-ASCA Comparison*

Figure 6 permits a direct comparison of the *ROSAT* and *ASCA* spectra for the six sources in common to the instruments. We have superposed a histogram of the best single-temperature low-abundance model on each *ASCA* spectrum (*left-hand panel*). This astrophysical model, including its *ASCA* normalization, has been convolved through the *ROSAT* telescope and PSPC response functions and is plotted on each PSPC spectrum (*right-hand panel*). In four cases, the shapes of the *ASCA* and *ROSAT* spectra are reasonably close, with major differences seen only in normalization and at $\lesssim 0.5$ keV, where *ASCA* provides little

TABLE 6

PARAMETERS FROM SPECTRAL FITS: *ASCA*

| *ASCA* Source | $I$ | Circle Size[a] | Energy (keV) | log $N_H$ ($cm^{-2}$) | $kT_1$ (keV) | Error (keV) | $kT_2$ (keV) | Error (keV) | $Norm_1$ ($10^{-18}$ $cm^{-5}$) | Error ($10^{-18}$ $cm^{-5}$) | $Norm_2$ ($10^{-18}$ $cm^{-5}$) | Error ($10^{-18}$ $cm^{-5}$) | $F_X$[b] | $\chi^2$ |
|---|---|---|---|---|---|---|---|---|---|---|---|---|---|---|
| 1 ..... | G2 | c | 0.8–3.0 | 20.6 | 0.8 | 0.1 | ... | ... | 39.0 | 17.9 | ... | ... | 9.8 | 0.7 |
| | | | | 20.6 | 0.6 | 0.2 | 1.4 | 0.5 | 2.1 | 1.1 | 6.3 | 1.4 | 10.1 | 0.9 |
| 2 ..... | S0 | b | 0.5–5.0 | 21.3 | 2.3 | 0.2 | ... | ... | 46.8 | 3.5 | ... | ... | 27.0 | 1.3 |
| | | | | 21.2 | 1.0 | 0.1 | 4.7 | 1.0 | 2.4 | 1.9 | 22.4 | 1.7 | 27.5 | 1.8 |
| 3 ..... | S0 | a | 0.5–2.5 | 20.5 | 0.8 | 0.1 | ... | ... | 12.6 | 1.9 | ... | ... | 4.9 | 0.6 |
| | | | | 20.5 | 0.8 | 0.1 | 4.8 | 3.1 | 1.0 | 0.4 | 3.0 | 0.8 | 4.7 | 0.9 |
| 4 ..... | S0 | b | 0.5–3.0 | 20.7 | 1.0 | 0.4 | ... | ... | 34.8 | 3.1 | ... | ... | 15.8 | 1.4 |
| | | | | 20.7 | 0.8 | 0.1 | 4.1 | 0.9 | 3.3 | 0.6 | 10.5 | 0.8 | 15.8 | 1.2 |
| 4(f)..... | S0 | b | 0.5–3.0 | 20.7 | 1.9 | 0.5 | ... | ... | 78.3 | 11.0 | ... | ... | 43.9 | 1.2 |
| 4(nf)..... | S0 | b | 0.5–2.5 | 20.7 | 0.9 | 0.1 | ... | ... | 19.2 | 2.1 | ... | ... | 8.0 | 1.6 |
| 5 ..... | G2 | c | 0.8–3.5 | 20.8 | 1.1 | 0.1 | ... | ... | 5.9 | 8.1 | ... | ... | 4.5 | 0.7 |
| 6 ..... | S0 | a | 0.5–2.5 | 21.2 | 2.4 | 1.7 | ... | ... | 5.6 | 3.1 | ... | ... | 3.9 | 1.1 |
| | | | | 20.7 | 0.6 | 0.2 | 3.2 | 1.1 | 0.2 | 0.3 | 4.3 | 0.8 | 4.0 | 0.9 |
| 7 ..... | G2 | d | 0.8–5.0 | 20.6 | 1.2 | 0.2 | ... | ... | 38.1 | 16.7 | ... | ... | 21.5 | 1.0 |

[a] a = 1.'5; b = 2'; c = 4.'00; d = 4.'25.
[b] $F_X$ in units of $10^{-13}$ ergs $s^{-1}$ $cm^{-2}$.

TABLE 7

*ROSAT* OBSERVATION INTERVALS

| Interval | Day (1993) | Start (UT) | End (UT) |
|---|---|---|---|
| a ..... | Feb 21 | 21:13 | 21:37 |
| b ..... | Feb 24 | 06:15 | 06:31 |
| c ..... | Feb 24 | 09:23 | 10:08 |
| d ..... | Feb 24 | 11:00 | 11:48 |

information. The principal exception is the CTT star XZ Tau (L1551X 19 = *ASCA* source 2), which is very faint in the *ROSAT* image but the dominant source with a very hard spectrum in the *ASCA* image. V826 Tau (L1551X 26 = *ASCA* 4) is brighter in the *ASCA* observation because of a flare event (§ 6).

## 5. TIMING ANALYSIS

We search for the presence of X-ray variability using three statistical tests: the Kolmogorov-Smirnov (K-S) test, which measures the maximum deviation of the integral photon arrival times from a constant source model; the Cramer–von Mises (CvM) test, which measures the sum of the square deviations between the integral arrival times and a constant source model; and the chi-squared ($\chi^2$) test, which measures the sum of the square deviations of binned count rates from the mean intensity. Each test should be sensitive to different types of variable behavior. For instance, the K-S and $\chi^2$ tests should be sensitive to secular changes, the K-S test might be most sensitive to brief flares, and the CvM test should be sensitive to pulsations or stochastic variability around the mean. The contribution of background variability is ignored. Analysis was based on IRAF/PROS software for *ROSAT* and XANADU/XRONOS (version 4.02) software for *ASCA*.

The PSPC observed the L1551 region for one satellite orbit on 1993 February 21, one orbit early on February 24, and two consecutive orbits later the same day. The starting and ending times for these four intervals are given in Table 7. Table 8 gives the variability tests results, and mean count rate during the four orbits, for the 11 L1551X sources that are inconsistent with a constant source at a significance level $P < 0.05$ in one or more test. The integral distributions of photon arrival times for these sources, with the constant source model shown as dotted lines, are plotted in Figure 7. Interpretation of the variability is complicated by the purposeful "wobbling" of *ROSAT*'s pointing with ~400 s period, which modulates sources near the support structure. This effect is seen most clearly as ripples in the light curve of source 14 in Figure 7. But this effect should not be responsible for the long-term variations seen in other sources.

The range of PSPC count rates for most of the variable sources is less than a factor of 2 over timescales of a few thousand seconds. The more dramatic changes include a drop from 81 to 38 counts $s^{-1}$ within 1 hr in the CTT binary UX Tau (L1551X 7) and a rapid increase in the last few minutes observed in the Hyad HZ 9 (L1551X 27). These findings are consistent with past studies of T Tauri X-ray variability (see, e.g., Montmerle et al. 1983; Strom & Strom 1994).

*ASCA* observed the L1551 cloud for 18 consecutive orbits spanning 27 hr. The probabilities that the source is variable, obtained from the $\chi^2$ and Kolmogorov-Smirnov tests of timing analysis, are given in the last two columns of Table 8. Of the seven *ASCA* sources, six are variable at a confidence level $P < 0.05$. They include three sources that were found to be variable by *ROSAT* and three that were not. The most dramatic instance of variability is the large flare on the WTT star V826 Tau, L1551X 26 = *ASCA* source 4, discussed in the next section.

Variations over the 1 yr separation between the *ROSAT* and *ASCA* observations can be sought by comparing normalizations of spectral fits in a fixed energy range. Figure 6 shows that XZ Tau (L1551X 19 = *ASCA* source 2), the strongest *ASCA* source, increased by a factor $\simeq 15$ in the 0.5–2.0 keV band between the observations from $\sim 1 \times 10^{-13}$ to $15.1 \times 10^{-13}$ ergs $s^{-1}$ $cm^{-2}$. This is comparable to the largest reported long-term variations in a T Tauri star (Walter & Kuhi 1984). There is no evidence for short-term flaring on XZ Tau within either observation. Figure 8*a* shows a completely featureless light curve during high state throughout the 26 hr *ASCA* observation.

## 6. FLARE ON V826 TAU

The light curve of V826 Tau, a spectroscopic binary T Tauri star with a $P = 3\overset{d}{.}8878$ period first discovered in *Ein-*

TABLE 8

SOURCES EXHIBITING VARIABILITY

| | *ROSAT* VARIABILITY PROBABILITY | | | *ROSAT* COUNT RATE (counts $ks^{-1}$) | | | | *ASCA* VARIABILITY PROBABILITY | |
|---|---|---|---|---|---|---|---|---|---|
| L1551X SOURCE | K-S Test | CvM Test | $\chi^2$ Test | a (1209 s) | b (964 s) | c (2687 s) | d (2864 s) | K-S Test | $\chi^2$ Test |
| 1 ..... | 99% | 99% | 99% | 84 ± 12 | 95 ± 14 | 116 ± 9 | 134 ± 9 | ... | ... |
| 7 ..... | 90 | 90 | >99 | 28 ± 6 | 45 ± 8 | 81 ± 6 | 39 ± 4 | ... | ... |
| 9 ..... | 90 | 90 | >99 | 14 ± 4 | 41 ± 8 | 39 ± 4 | 38 ± 4 | ... | ... |
| 14 ..... | 99 | 99 | >99 | 149 ± 11 | 90 ± 10 | 79 ± 6 | 72 ± 5 | 70.0% | 80.0% |
| 18 ..... | 99 | 99 | 80 | 74 ± 8 | 59 ± 8 | 55 ± 5 | 61 ± 5 | ... | ... |
| 19 ..... | ... | ... | ... | ... | ... | ... | ... | 98.0 | 99.7 |
| 24 ..... | ... | ... | ... | ... | ... | ... | ... | 20.0 | 99.4 |
| 25 ..... | 95 | 95 | 95 | 55 ± 8 | 52 ± 8 | 46 ± 5 | 68 ± 5 | 96.0 | 96.0 |
| 26 ..... | 99 | 99 | >99 | 135 ± 11 | 98 ± 10 | 79 ± 6 | 95 ± 6 | >99.9 | >99.9 |
| 27 ..... | 99 | 99 | 98 | 35 ± 6 | 25 ± 6 | 19 ± 3 | 32 ± 4 | ... | ... |
| 32 ..... | ... | ... | ... | ... | ... | ... | ... | 98.0 | >99.9 |
| 33 ..... | 95 | 95 | 98 | 10 ± 5 | 12 ± 6 | 15 ± 4 | 1 ± 3 | ... | ... |
| 35 ..... | 99 | 95 | >99 | 252 ± 15 | 181 ± 14 | 173 ± 8 | 214 ± 9 | 87 | 99.9 |
| 37 ..... | 90 | 95 | 30 | 14 ± 9 | 16 ± 11 | 16 ± 6 | 9 ± 5 | ... | ... |

1996ApJ...464..286C

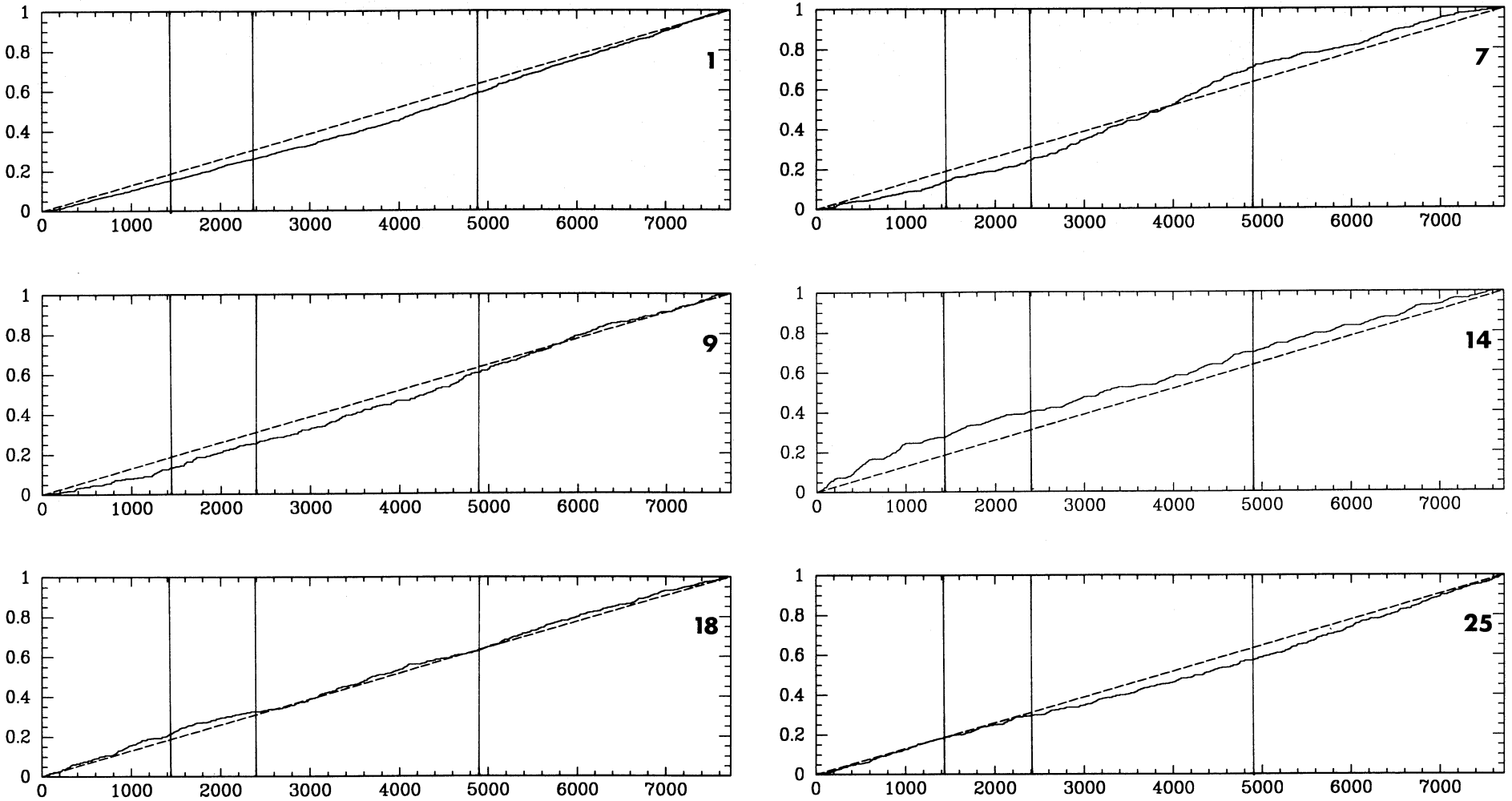


FIG. 7.—Integrated normalized distribution of photon arrival times as a function of detector on-time in seconds (*solid curves*) for 11 variable *ROSAT* sources (Table 8). The diagonal dashed lines represent the expected distribution for a constant source with the observed mean count rate. The vertical lines demarcate the four observation intervals.

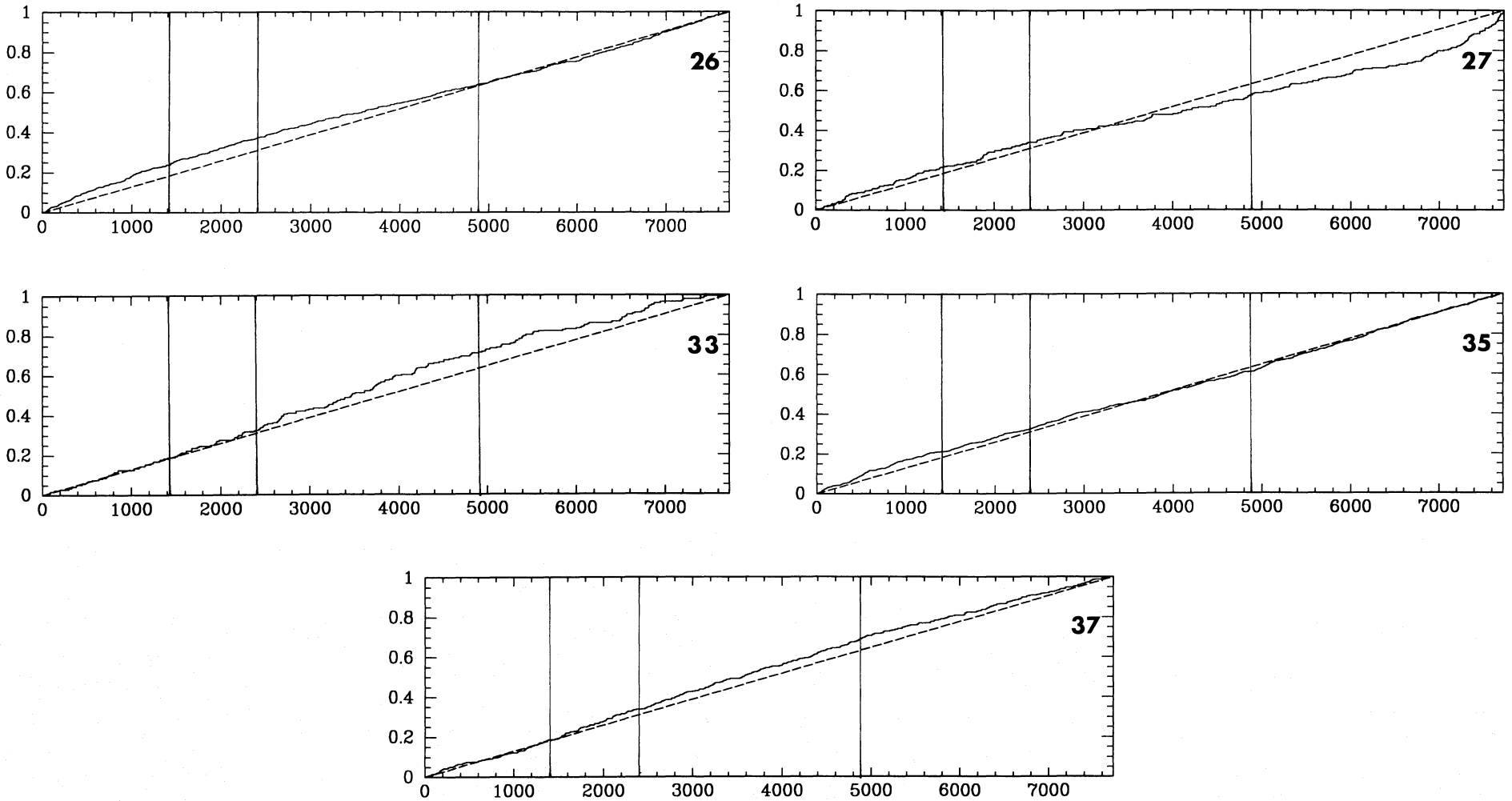


FIG. 7—*Continued*

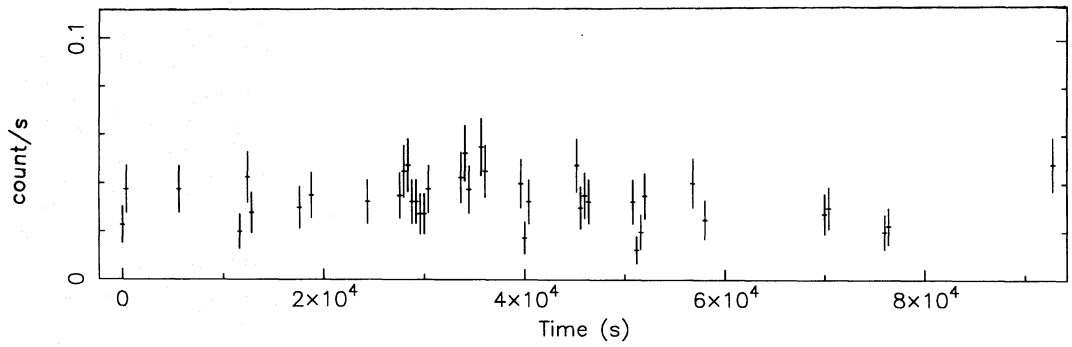


FIG. 8*a*

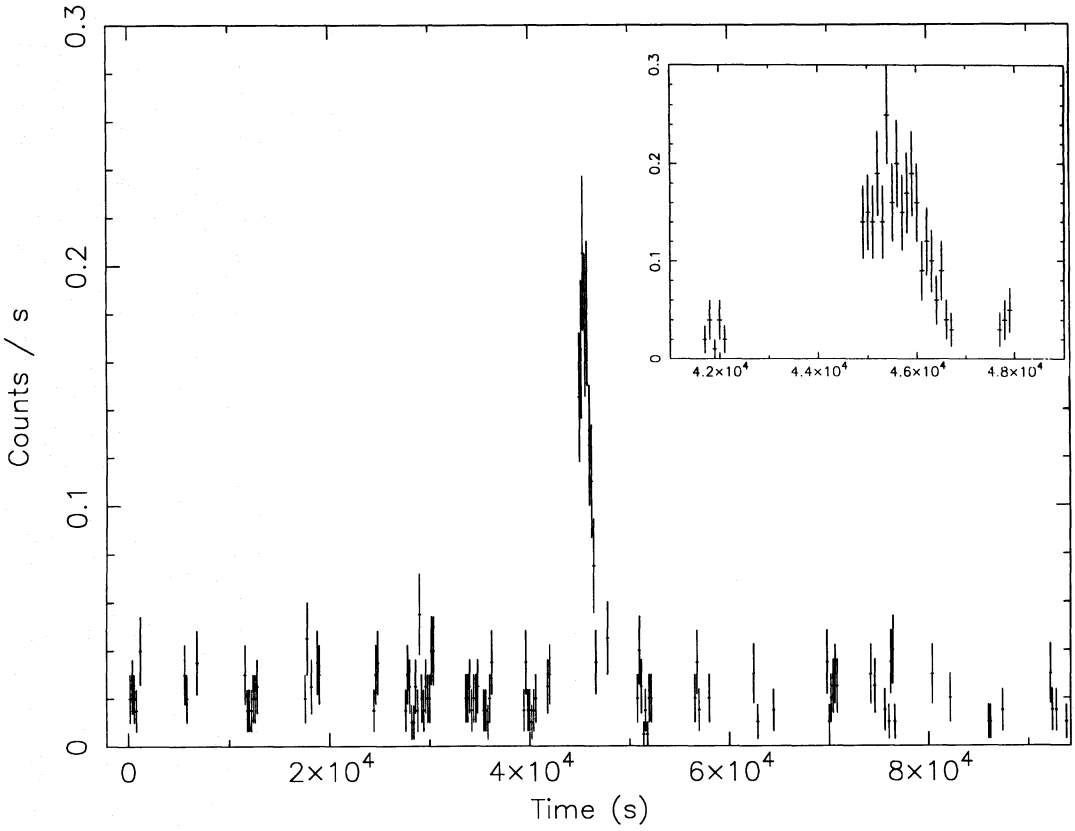


FIG. 8*b*

FIG. 8.—(*a*) *ASCA* GIS2 light curve of XZ Tau, using 400 s bins. Time is in seconds from the beginning of observation. (*b*) *ASCA* GIS2 light curve of V826 Tau. The main panel has 200 s bins, while the inset showing the flare has 100 s bins.

*stein* X-ray images (Feigelson & DeCampli 1981; Reipurth et al. 1990), shows a large flare during the *ASCA* observation (Fig. 8*b*). The excess extends for 2200 s starting about 44,700 s into the observation, but the flare probably began a few hundred seconds earlier during Earth blockage. The flare has a peak count rate of 0.2 GIS counts per second, as compared with the average quiescent rate of approximately 0.05 counts $s^{-1}$. The quiescent levels were constant for 12 hr before and after the flare event. Applying the average spectrum given in Table 6, the average luminosity of the flare over the range 0.5–5 keV is $1.0 \times 10^{31}$ ergs $s^{-1}$, compared with the average quiescent luminosity of $1.9 \times 10^{30}$ ergs $s^{-1}$. If it is assumed that the flare is temporally symmetrical, the total energy in the flare is $\sim 3 \times 10^{34}$ ergs. Figure 9 shows spectra of V826 Tau during the flare and the quiescent phases. A one-temperature Raymond-Smith plasma fits both levels, with the flare at $1.9 \pm 0.5$ keV and the quiescent emission at $0.9 \pm 0.1$ keV.

The flare on V826 Tau is roughly comparable in behavior to those seen on other T Tauri stars (e.g., DG Tau and DD Tau; Feigelson & DeCampli 1981). The flare is $10^2$ times more energetic than the most powerful solar flares (Kane et al. 1995) but has $10^2$ less total energy than the strongest T Tauri events (e.g., ROX 20—Montmerle et al. 1983; LkHα 92—Preibisch, Zinnecker, & Schmitt 1993). A temperature near 2 keV ($1–2 \times 10^7$ K) is consistent with flares from a variety of sources including the Sun, dMe stars, and other T Tauri stars.

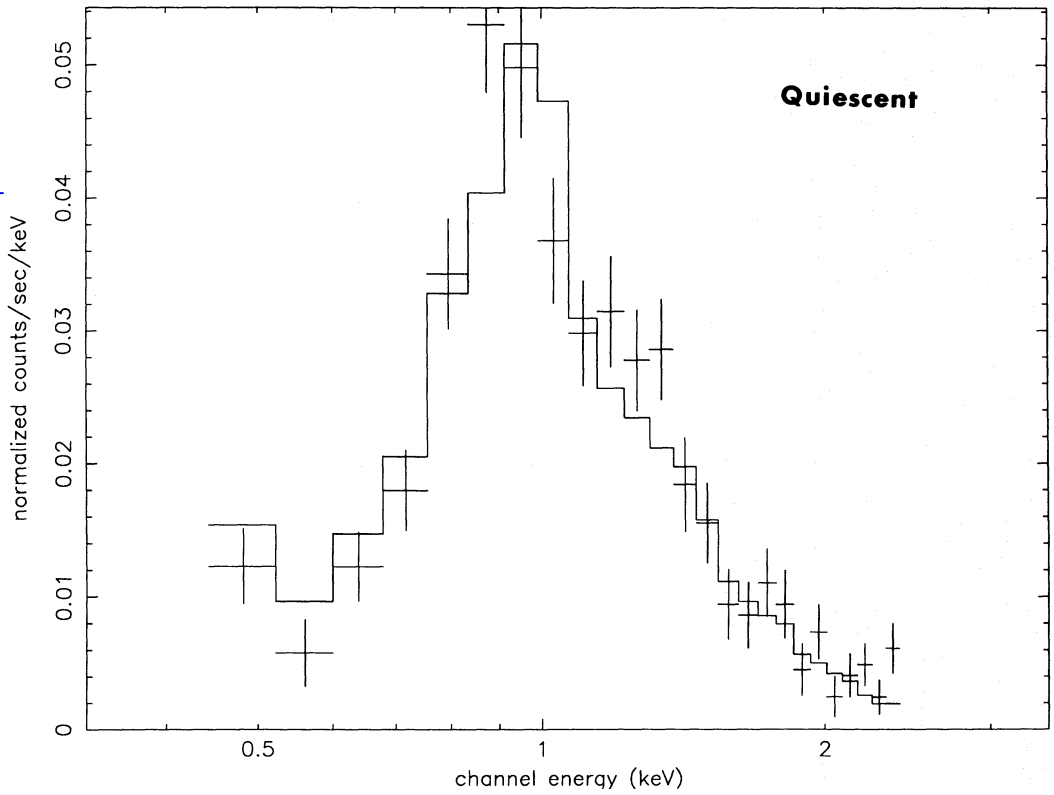


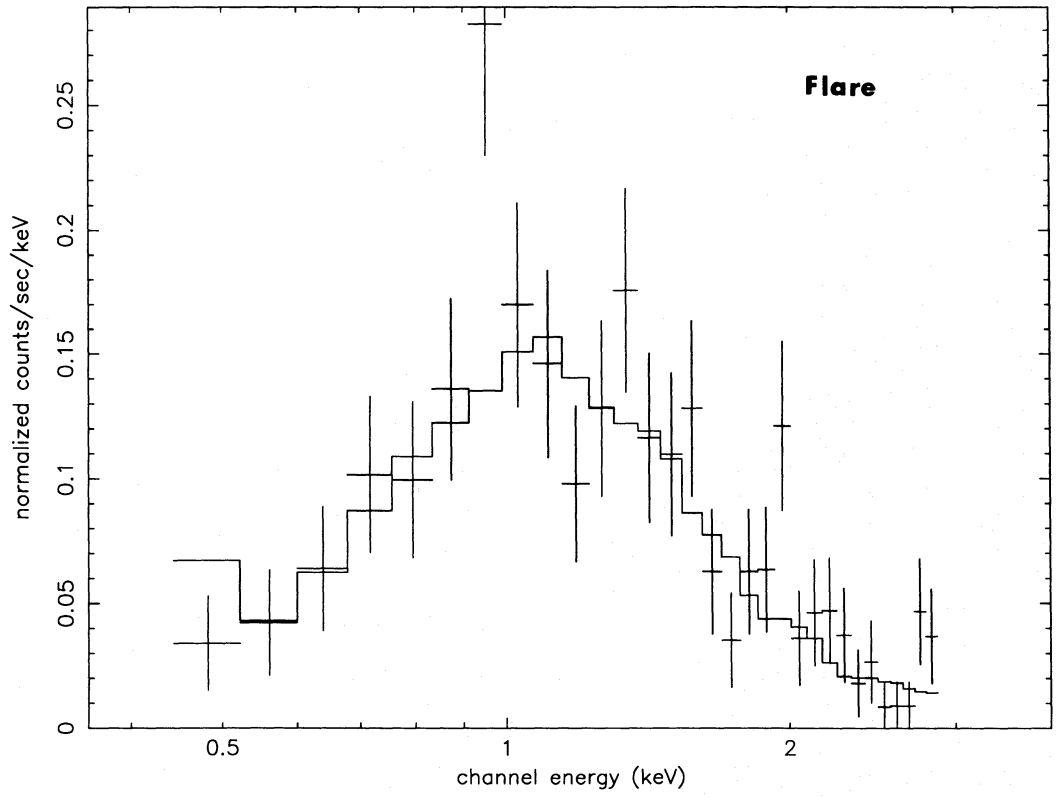


FIG. 9.—*ASCA* SIS0 spectra of V826 Tau, quiescent (*top panel*) and flare (*bottom panel*). Parameters for the model, shown in the histogram, are given in Table 6.

## 7. DISCUSSION

### 7.1. *Cloud Membership*

In addition to detecting seven of 12 previously identified T Tauri stars in the L1551 cloud, the *ROSAT* observation also detected 14 potential new T Tauri stars. The existing census of cloud members thus could be quite incomplete. A variety of diagnostics provide clues to cloud membership: Hα and Li 6707 Å spectral features, proper motion, radial velocity, photometry, and X-ray hardness ratios. Based on the data available to us (§ 3.2), we conclude that five of these stars are nonmembers (L1551X 1, 3, 12, 17, and 29), two are members (15 and 33), one may be a post–T Tauri star (20), and six have insufficient data to make a determination (8, 28, 30, 34, 36, and 37).

This detection rate is lower than previous optical identification surveys of "New" *ROSAT* sources in star-forming regions, where most of the unidentified X-ray sources are confirmed as new WTT stars (Huenemoerder et al. 1994; Alcalá-Estrada 1994). The large population of non–T Tauri X-ray sources in the L1551 field may be due to the presence of several overlapping stellar clusters: the Pleiades, the Hyades, and the Cas-Tau group. The Hyades and the Pleiades have proper motions that differ by about $0''.1\ \mathrm{yr}^{-1}$ from the mean of L1551 cloud members and can be readily distinguished in most cases. However, the kinematics of the Cas-Tau group and the Taurus clouds are nearly the same (Walter & Boyd 1991). The Cas-Tau group is an OB association of age about $3–5 \times 10^7$ yr at a distance of 150–200 pc, although both values are uncertain (Blaauw 1956, 1984). It is possible that some of our new or possible new sources, such as L1551X 20, which lies near the main sequence, are in fact low-mass members of this group.

The possibility that between two and nine new T Tauri stars may be present in the *ROSAT* image may impact the census of cloud members and thus the inferred initial mass function. The L1551 cloud vicinity has been carefully searched for Hα emission stars (Cudworth & Herbig 1979; Feigelson & Kriss 1983), Ca II emission stars (Herbig, Vrba, & Rydgren 1986), $11 < V < 17$ stars with proper motions consistent with the cloud (Jones & Herbig 1979; Gomez et al. 1992), and *Einstein* X-ray emission stars with a luminosity limit of $\simeq 10^{30.0}$ ergs $\mathrm{s}^{-1}$ (Feigelson et al. 1987; Strom et al. 1990). These surveys uncovered a total of 12 T Tauri stars associated with the cloud.

Positive identification of the new *ROSAT* objects will help to improve the survey of T Tauri stars in L1551. Although we do not have enough information to calculate a new initial mass function, at least one of our new stars (L1551X 33) appears to be an M star. This is consistent with the results of Strom & Strom (1994) in L1495E, who find several low-mass T Tauri M stars in a deep *ROSAT* exposure. The detection of these objects helps to alleviate the deficiency of low-mass stars in previous initial mass functions.

There still remains a potentially serious problem in our census of L1551 stars: Are all the T Tauri stars formed by the L1551 cloud within the fields of these surveys? Recent evidence from the *ROSAT* All-Sky Survey suggests T Tauri stars can be found as far as 10°–20° away from star-forming regions (Alcalá-Estrada 1994; Neuhäuser et al. 1995b). A spatial dispersion of T Tauri stars may also explain the lack of older (age ≥ than few million years) stars in past T Tauri samples (Hartmann et al. 1991; Feigelson 1996). If star formation has proceeded for longer than a few million years, the number of young stars in each age group should be the same. Since this is not seen, either L1551 is in a short-lived starburst phase or many of its older stars have moved away from the cloud. The result of this dispersal of T Tauri stars is that surveys near active cloud cores like L1551, no matter how deep, will give only a partial census of star formation from the entire cloud complex (Feigelson 1996).

### 7.2. *X-Ray Spectral Analysis*

Spectral analysis of the T Tauri stars reveals spectra dominated by a 1 keV component. *ROSAT* spectra of foreground stars contain a similar peak at 1 keV as well a soft component at about 0.2 keV. This soft component may be present in T Tauri stars but masked by the intervening extinction. Simulations indicate that X-ray spectra of foreground stars resemble those of T Tauri stars if obscuration at levels of $\sim \log N_{\mathrm{H}} = 20$ is artificially added. It is not clear whether meaningful physical differences exist between sources characterized by one- and two-temperature models. It is important to remember that the model temperatures are parameterizations and do not necessarily indicate discrete emitting regions at two distinct temperatures. *ASCA* spectra are also dominated by a 1 keV component. *ASCA*'s poor energy sensitivity at less than ~0.5 keV makes it difficult to confirm the soft component seen by *ROSAT*. Two-temperature fits to the *ASCA* data indicate a hard component (~2–5 keV) may be present in some sources.

Two-temperature Raymond-Smith plasmas provide the best fit to several types of coronally active stars; for example, *ROSAT* observations of RS CVn binaries are also well fitted by plasma at ~0.2 and ~1.0 keV (Dempsey et al. 1993). A cooling curve analysis may explain these temperatures in terms of thermally stable states of coronal plasma. A model coronal plasma whose primary cooling mechanisms are bremsstrahlung and line emission produces thermally stable points near the temperatures commonly found for cool star coronae (Gehrels & Williams 1993).

Studies of magnetically active stars with *ASCA* have recently found relatively weak emission lines compared to those expected from a solar abundance plasma (see, e.g., Singh, Drake, & White 1995). We find best-fit spectral models with extremely low abundances (≃10% solar levels). It is quite possible that this is not a physically real effect, but rather an artifact of the omission of many emission lines from existing plasma emission models, such as the iron L-shell lines around 1.0–1.6 keV (Liedahl, Osterheld, & Goldstein 1995). We also have not considered models with enhanced abundances of elements according to their first ionization potential (FIP). Since our data cannot distinguish between two-temperature and single-temperature low-abundance models with statistical significance and since the low-abundance fits may be an artifact of poor plasma modeling, we do not place much scientific value on the details of the spectral results.

### 7.3. *Variability*

As in *Einstein Observatory* studies (see, e.g., Montmerle et al. 1983), most T Tauri stars in L1551 exhibit variability on timescales of a day or longer. Of seven previously known cloud members detected, only one (V710 Tau) was not seen to vary. Three dramatic changes were seen: a factor of 15 rise in the extremely young CTT XZ Tau over 1 year, a factor of 2 fall in the CTT star UX Tau in 1 hr, and a factor

of 5 rise and fall in $\simeq 40$ minutes in the WTT spectroscopic binary V826 Tau. L1551X 33, a likely "New" T Tauri star, and the luminous pre–main-sequence B star HD 28867 are variable as well.

The flare on the X-ray-discovered WTT star V826 Tau has excellent temporal and spectral coverage. It shows, more clearly than any previous X-ray observation of a T Tauri star, distinct "flare" and "quiescent" components. The constant level at $2 \times 10^{30}$ ergs $s^{-1}$, though very strong compared to quiescent solar levels, is virtually constant for 24 hr. The flare, 30–60 minutes long with peak luminosity 5 times the quiescent level, did not produce any enhancement or change in the quiescent level. This strongly suggests geometrically heterogeneous emission regions, either a corona–plus–active region configuration on one star, or a corona on one star and the flare on its companion. Spectral analysis indicates that the flare plasma is $\sim 1$ keV hotter than the quiescent, consistent with other flare observations (see, e.g., Montmerle et al. 1983; Preibisch et al. 1993).

### 7.4. *Individual Sources*

XZ Tau (L1551X 19, *ASCA* 2) is an extremely young and active CTT star (age $\sim 55{,}000$ yr; Beckwith et al. 1990). It is an infrared source and powers a molecular outflow. While studies of the environment of XZ Tau are complicated by its proximity to HL Tau 30″ away, *ROSAT* clearly resolves XZ Tau as the X-ray source. XZ Tau is unusual in being both the hardest object in the *ASCA* field (one-temperature Raymond-Smith plasma at about 2.3 keV) and the only object to vary by large factors between the *ROSAT* and *ASCA* observations. The hard emission seen with *ASCA* cannot be due to a rapid flare (Fig. 8*a*), as seen in V826 Tau (Fig. 8*b*), because no flux change was detected over the 26 hr duration of the observation. A possible interpretation is a two-component X-ray spectrum: a soft thermal component from the star itself, and a high-energy power-law component produced in high-speed shocks in the jet. The variability of the source may be a result of an episodic nature of the outflow. Alternatively, the hard component may arise from magnetic reconnection at the base of the outflow, rather than near the stellar surface where WTT X-ray emission is produced. Flaring might occur where the stellar magnetic field strongly interacts with the circumstellar disk near the corotation radius (Shu et al. 1994).

The X-ray properties of the 6th mag pre–main-sequence B9 star HD 28867 = HR 1442 are surprisingly similar to those of the low-mass T Tauri stars. Its ratio of X-ray to optical emission is 2 orders of magnitude above those of main-sequence B stars (Walter & Boyd 1991). It is one of a number of pre–main-sequence B and A stars with strong X-ray emission (Walter et al. 1988). The cause of this excess is not well understood, as these stars are believed to lack the outer convection zones necessary for the dynamo model to generate magnetic fields (Caillault & Zoonematkermani 1989). Two explanations suggest themselves: HD 28867 has a low-mass WTT companion, which produces the X-rays; or fossil magnetic fields inherited from the cloud before star formation, rather than dynamo fields, are responsible for the magnetic activity. There are also models for X-ray emission from A and B stars that involve nonmagnetic phenomena, such as wind-driven shocks (e.g., Cassinelli et al. 1994).

L1551 is well known for its outflows and Herbig-Haro objects. No emission was detected by either *ROSAT* or *ASCA* from any flow region, including the prominent outflow complex associated with L1551 IRS 5. This is consistent with previous X-ray studies of protostellar outflows.

L1551 contains the two brightest infrared sources in the Taurus clouds; L1551 IRS 5 and L1551NE. Both have Class I infrared spectra, indicating they are surrounded by a dusty envelope (Moriarty-Schieven, Butner, & Wannier 1995). These objects, along with the HL/XZ Tau group, are responsible for powering the complex of outflows and Herbig-Haro objects in the field (Moriarty-Schieven et al. 1994, 1995). There is reason to expect embedded protostars to be X-ray sources. *ROSAT* observations of $\rho$ Ophiuchi (Casanova et al. 1995) may have detected such emission, but because of the crowded field source identification is difficult. Protostellar X-ray emission may also be necessary to ionize protostellar outflows. The nondetection of L1551 IRS 5 and L1551NE may indicate a lack of X-ray emission from the protostars or may also be the result of large amounts of obscuration. $N_H$ values of $\sim 1 \times 10^{23}$ would prevent detection of a object with a similar luminosity to the WTT stars in field. Both L1551 IRS 5 and L1551NE have very massive envelopes (0.14 and 0.042 $M_\odot$) inferred from infrared and millimeter data (Moriarty-Schieven et al. 1994), and, since the L1551 IRS 5 outflow is in a plane roughly perpendicular to the line of sight, it is quite possible that X-ray emission is being absorbed in the accretion disk around the protostar. L1551NE may be a Class 0 source, a very young protostar that has not yet accreted the bulk of its matter (Moriarty-Schieven et al. 1995; André & Montmerle 1994).

## 8. CONCLUSIONS

Combining *ROSAT* and *ASCA* observations yields unique information on T Tauri star X-ray emission over both a large spectral range and spatial area. *ROSAT*'s large field of view and high spatial resolution allows X-ray sources to be identified with known T Tauri stars and potential new T Tauri stars. Its sensitivity below 0.5 keV provides for analysis of a soft emission component and foreground absorption. *ASCA*'s high spectral resolution and wide bandpass allow for detailed modeling of the X-ray spectra and imaging deep into highly obscured regions of the molecular cloud. Combining our X-ray data with optical observations and proper-motion studies yields these conclusions:

1. The *ROSAT* image contains 38 X-ray sources; two to three are CTT stars, five to seven are previously known WTT stars, two are new T Tauri stars, five are possible new T Tauri stars, one is the active B9e star HD 28867, three have too little information to make a determination, and 21 are stars or extragalactic sources unrelated to the cloud. The rate of detection of new WTT stars is significantly lower than surveys of other star-forming regions, which suggests that the census of T Tauri stars in the L1551 field is nearly complete. Many of the non–T Tauri X-ray stars are young main-sequence stars unrelated to the cloud, including Hyads and possibly members of the Cas-Tau association. Our goal of completing the survey of T Tauri stars in the region is hindered by the possibility that some cloud members have dispersed from the immediate vicinity of the cloud.

2. Both *ROSAT* and *ASCA* spectra can be fitted by two-temperature plasmas and by a single-temperature plasma with low abundance of elements with respect to the solar

photosphere. While two-temperature models provide a good fit to many active stars and stellar coronal abundances probably differ from solar photospheric, we conclude that the lack of completeness of the model plasma codes prevents definitive statements about the detailed plasma properties.

3. Timing analysis indicates that all but one of the observed T Tauri stars are variable in one or both observations. A dramatic flare is seen on the WTT star V826 Tau, lasting about 3000 s with a average soft X-ray luminosity of $\sim 1 \times 10^{31}$ ergs $s^{-1}$. A quiescent component with luminosity around $2 \times 10^{30}$ ergs $s^{-1}$ was unaffected by the flare event.

4. No X-ray emission is detected from any of the Herbig-Haro objects or outflows in the region. X-rays are not detected from the Class 0/1 protostars L1551 IRS 5 or L1551NE, the two strongest infrared sources in the Taurus clouds.

5. The CTT XZ Tau shows unusual behavior in the observations. It is the hardest source in the *ASCA* observation and increases in flux by a factor of 15 between the *ROSAT* and *ASCA* observations. XZ Tau is an extreme CTT star with a prominent disk and associated outflows. We suggest that the increase in luminosity and the *ASCA* spectrum may arise in outflow shocks or at the base of the outflow.

The authors would like to thank Dave Burrows for providing the *ROSAT* data. The referee, Marc Gagné, provided many useful comments. This work was based partially on observations obtained with the Palomar 1.5 m telescope, which is operated jointly by the California Institute of Technology and the Observatories of the Carnegie Institution of Washington. Portions of this work were supported by NASA grants NAG 5-2527 and NAGW-2120. We would also like to thank the Space Telescope Science Institute for providing us with access to the digitized Palomar Sky Survey. This research has made use of the SIMBAD database, operated at CDS, Strasbourg, France.

## REFERENCES

Alcalá-Estrada, 1994, Ph.D. thesis, Ruprecht Karls Universität, Heidelberg
André, P., & Montmerle, T. 1994, ApJ, 420, 837
Appenzeller, I., & Mundt, R. 1989, Astron. Astrophys. Rev., 1, 291
Beckwith, S. V. W., Sargent, A. I., Chini, R. S., & Gusten, R. 1990, AJ, 99, 924
Bertout, C. 1989, ARA&A 27, 351
Blaauw, A. 1956, ApJ, 123, 408
———. 1984, in The Milky Way Galaxy, ed. H. van Woerdel, R. J. Allen & W. B. Burton (Dordrecht: Reidel), 335
Caillault, J.-P., & Zoonematkermani, S. 1989, ApJ, 338, L57
Casanova, S., Montmerle, T., Feigelson, E. D., & André, P. 1995, ApJ, 439, 752
Cassinelli, J. P., Cohen, D. H., MacFarlane, J. J., Sanders, W. T., & Welsh, B. Y. 1994, ApJ, 421, 705
Cruddace, R. G., Hasinger, G. R., & Schmitt, J. H. M. M. 1988, in ESO Conference and Workshop Proc. 28, Astronomy from Large Databases, ed. F. Murtagh & A. Heck (Garching: ESO), 177
Cudworth, K. M., & Herbig, G. 1979, AJ, 84, 548
Dempsey, R. C., Linsky, J. L., Schmitt, J. H. M. M., & Fleming, T. A. 1993, ApJ, 413, 333
Feigelson, E. D. 1996, in preparation
Feigelson, E. D., Casanova, S., Montmerle, T., & Guibert, J. 1993, ApJ, 416, 623 (FCMG)
Feigelson, E. D., & DeCampli, W. M. 1981, ApJ, 243, L89
Feigelson, E. D., Giampapa, M. S., & Vrba, F. J. 1991, in The Sun in Time (Tucson: Univ. of Arizona Press), 658
Feigelson, E. D., Jackson, J. M., Mathieu, R. D., Myers, P. C., & Walter, F. M. 1987, AJ, 94, 1251
Feigelson, E. D., & Kriss, G. A. 1981, ApJ, 248, L35
———. 1983, AJ, 88, 431
———. 1989, ApJ, 338, 262
Gagné, M., & Caillault, J.-P. 1994, ApJ, 437, 361
Gehrels, N., & Williams, E. D. 1993, ApJ, 418, L25
Gomez, M., Jones, B. F., Hartmann, L., Kenyon, S. J., Stauffer, J. R., Hewett, R., & Reid, I. N. 1992, ApJ, 104, 762
Hartigan, P., Strom, K. M., & Strom, S. E. 1994, ApJ, 427, 961.
Hartmann, L., Jones, B. F., Stauffer, J. R., & Kenyon, S. J. 1991, AJ, 101, 1050
Herbig, G. H., & Bell, K. R. 1988, Lick Obs. Bull, 1111 (HBC)
Herbig, G. H., Vrba, R. J., & Rydgren, A. E. 1986, AJ 91, 575.
Huenemoerder, D. P., Lawson, W. A., & Feigelson, E. D. 1994, MNRAS, 271, 967
Jones, B. F., & Herbig, G. 1979, AJ 84, 1872.
Joy, A. H. 1942, PASP, 54, 15
Kane, S. R., Hurley, K., McTiernan, J. M., Sommer, M., Boer, M., & Niel, M. 1995, ApJ, 446, L47
Kenyon, S. J., Dobrzycka, D., & Hartmann, L. 1994, AJ, 108, 1872
Koyama, K. 1987, PASJ, 39, 245
Koyama, K., Asoka, I., Kuriyama, T., & Tawara, Y. 1992, PASJ, 44, L255
Koyama, K., Maeda, Y., Ozaki, M., Ueno, S., Kamata, Y., Tawara, Y., Skinner, S., & Yamauchi, S. 1994, PASJ, 46, L125
Liedahl, D. A., Osterheld, A. L., & Goldstein, W. H. 1995, ApJ, 438, L115
Luyten, W. J. 1971, The Hyades (Minneapolis: Univ. of Minnesota)
MacGillivray, H. T., & Stobie, R. S. 1984, Vistas Astron., 27, 433
Montmerle, T., Feigelson, E. D., Bouvier, J., & André, P. 1993, in Protostars and Planets III, ed. E. H. Levy & J. I. Lunine (Tucson: Univ. Arizona Press), 689
Montmerle, T., Koch-Miramond, L., Falgarone, E., & Grindlay, J. E. 1983, ApJ, 269, 182
Moriarty-Schieven, G. H., Butner, H. M., & Wannier, P. G. 1995, ApJ, 445, L55
Moriarty-Schieven, G. H., & Snell, R. L. 1988, ApJ, 332, 364
Moriarty-Schieven, G. H., Wannier, P. G., Keene, J., & Tamura, M. 1994, ApJ, 436, 800
Morrison, R., & McCammon, D. 1983, ApJ, 270, 119
Neuhäuser, R., Sterzik, M. F., Schmitt, J. H. M. M., Wichmann, R., & Krautter, J. 1995a, A&A, 297, 391
Neuhäuser, R., Sterzik, M. F., Torres, G., & Martin, E. L. 1995b, A&A, in press
Oke, J. B., & Gunn, J. E. 1983, ApJ, 266, 713
Pallavicini, R., Golub, L., Rosner, R., Vaiana, G. S., Ayres, T., & Linsky, J. L. 1981, ApJ, 248, 279
Pfeffermann, E., et al. 1986, Proc. SPIE, 733, 519
Pravdo, S. H., & Marshall, F. E. 1981, ApJ, 248, 591
Preibisch, Th., Zinnecker, H., & Schmitt, J. H. M. M. 1993, A&A, 279, L33
Reid, N. 1990, MNRAS, 247, 70
———. 1992, MNRAS, 257, 257
———. 1993, MNRAS, 265, 85
Reipurth, B., Lindgren, H., Nordstrom, B., & Mayor, M. 1990 A&A, 235, 197
Reipurth, B. 1994, A General Catalogue of Herbig-Haro Objects, electronically published via anon. ftp to ftp.hq.eso.org, directory /pub/Catalogs/Herbig-Haro
Shu, F., Najita, J., Ostriker, E., Wilkin, F., Ruden, S., & Lizano, S. 1994, ApJ, 429, 781
Silk, J. 1995, ApJ, 408, L41
Silk, J., & Norman, C. 1985, ApJ, 293, 542
Singh, K. P., Drake, S. A., & White, N. E. 1995, ApJ, 445, 840
Stark, A. A., Gammie, C. F., Wilson, R. W., Bally, J., Linke, R. A., Heiles, C., & Hurwitz, M. 1992, ApJS 79, 77
Strom, K. M., et al. 1990, ApJ 362, 168
Strom, K. M., & Strom, S. E. 1994, ApJ, 424, 23
Tanaka, Y., Inoue, H., & Holt, S. S. 1994, PASJ, 46, L37
Walter, F. M., & Boyd, W. T. 1991, ApJ, 370, 318
Walter, F. M., Brown, A., Mathieu, R. D., Myers, P. C., & Vrba, F. J. 1988, AJ, 96, 297
Walter, F. M., & Kuhi, L. V. 1984, ApJ, 284, 194
Wood, K. S., et al. 1984, ApJS, 56, 507